

Provided for non-commercial research and education use.  
Not for reproduction, distribution or commercial use.



This article appeared in a journal published by Elsevier. The attached copy is furnished to the author for internal non-commercial research and education use, including for instruction at the authors institution and sharing with colleagues.

Other uses, including reproduction and distribution, or selling or licensing copies, or posting to personal, institutional or third party websites are prohibited.

In most cases authors are permitted to post their version of the article (e.g. in Word or Tex form) to their personal website or institutional repository. Authors requiring further information regarding Elsevier's archiving and manuscript policies are encouraged to visit:

<http://www.elsevier.com/copyright>



Contents lists available at ScienceDirect

Vision Research

journal homepage: [www.elsevier.com/locate/visres](http://www.elsevier.com/locate/visres)

## Texture modulation detection by probability summation among orientation-selective and isotropic mechanisms

Nicolaas Prins\*

Department of Psychology, University of Mississippi, Peabody Building, P.O. Box 1848, University, MS, 38677, USA

### ARTICLE INFO

#### Article history:

Received 16 March 2008  
Received in revised form 6 September 2008

#### Keywords:

Texture  
Second-order  
FRF mechanism  
Contrast

### ABSTRACT

Substantial evidence has accumulated for the notion that modulations of second-order properties in the visual scene are processed by mechanisms which detect contrast variations within narrow orientation/spatial frequency channels. It has also been suggested that mechanisms exist which detect contrast modulations across all orientations. Many naturally occurring texture variations (e.g., modulations in orientation and/or spatial frequency) involve simultaneous contrast modulations in multiple channels. Contrasting conclusions have been drawn regarding the manner in which the information carried in multiple channels is combined. In a series of two experiments it is shown that simultaneous contrast modulations in two narrow orientation bands are detected by three mechanisms, two of which detect contrast modulations within the modulated bands only, the third of which integrates contrast across orientations in order to detect modulations of overall contrast. The three mechanisms combine their efforts by probability summation.

© 2008 Elsevier Ltd. All rights reserved.

### 1. Introduction

Many natural surfaces are textured and much information regarding, for example, the slant or the 3-D shape of such surfaces can be derived by analyzing variations in image statistics in the retinal image (e.g., Cutting & Millard, 1984; Knil, 1998a, 1998b; Li & Zaidi, 2000; Li & Zaidi, 2001; Li & Zaidi, 2003; Rosas, Wichmann, & Wagemans, 2004). For example, a curve in a textured surface may lead to a gradient not only in luminance but also in the orientation content and spatial frequency content in the retinal image of the texture. It may come as no surprise then that much research has concentrated on the mechanisms by which the visual system detects such gradients.

It has been well-established how the visual system detects gradients in luminance (first-order gradients). As early as the retina, 'Ganglion' cells display a preference for luminance differences across space while being relatively unresponsive to absolute luminance. In primary visual cortex (V1), 'simple' cells continue to signal luminance gradients although, compared to retinal and geniculate cells, they are more selective with regard to the spatial distribution of light, displaying selectivity for orientation (Hubel & Wiesel, 1962) as well as spatial frequency (Campbell, Cooper, & Enroth-Cugell, 1969).

The mechanisms underlying detection of second-order gradients (changes in image properties other than luminance, such as local orientation or spatial frequency) however, are not understood

as well. Much evidence has accumulated for what I will refer to as Filter-Rectify-Filter (FRF) models (e.g., Graham & Sutter, 1998; Graham & Wolfson, 2004; Landy & Bergen, 1991; Malik & Perona, 1990). Though specific models differ in details, all such models consist of three stages. In the first stage, the image is filtered with a set of linear filters (such as simple cells), which are selective for specific orientations and spatial frequencies. This first stage is followed by a non-linear operation such as half-wave rectification. This non-linear operation is necessary to avoid cancellation of positive and negative responses. The rectified output of the linear filter responses is then filtered by a larger second filter. Any existing differences in contrast between texture regions within the range of orientations and spatial frequencies for which the first-stage filters are sensitive may be detected by such mechanisms. A number of studies indicate that the first-stage filters are tuned for orientation and spatial frequency (e.g., Dakin & Mareschal, 2000; Graham, Sutter, & Venkatesan, 1993; Jamar & Koenderink, 1985; Langley, Fleet, & Hibbard, 1996; Mareschal & Baker, 1998; Mareschal & Baker, 1999; Prins & Kingdom, 2002; Prins & Kingdom, 2006; Sutter, Sperling, & Chubb, 1995).

One disadvantage of the FRF approach is that activity in any given FRF mechanism may have arisen in a number of different stimulus contexts. Consider, for example, the orientation-modulated (OM) texture in Fig. 1a. The orientation in this texture is square-wave modulated (i.e., regions that differ in orientation content but that are both homogeneous internally are alternated). The modulation amplitude in this texture is relatively large (20°, peak-to-trough) and the two regions should easily segregate. In Fig. 1b, the spectral amplitude distribution across orientation is

\* Fax: +1 662 915 5398.

E-mail address: [nprins@olemiss.edu](mailto:nprins@olemiss.edu)

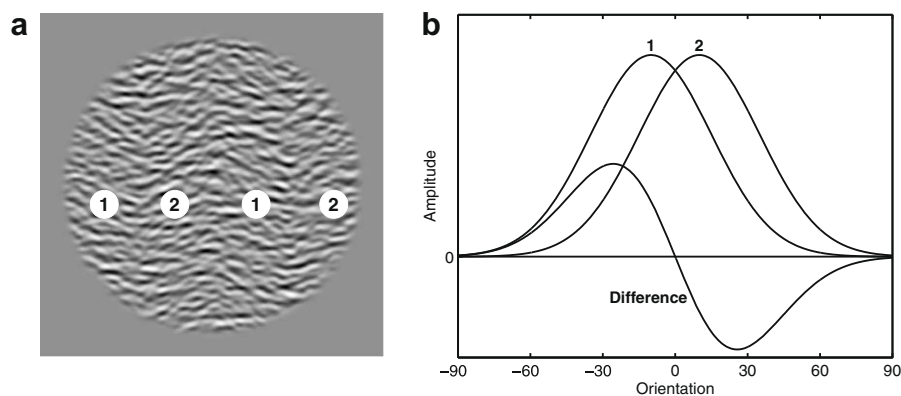


**Fig. 1.** (a) Orientation-modulated texture. The texture contains four vertical bars. Bars labeled 1 contain micropatterns centered on 10° clockwise from horizontal, while the micropatterns in bars labeled 2 are centered on 10° counterclockwise from horizontal. (b) Graphical representation of spectral distribution across orientation of the two different regions in the texture in this Figure. Also shown is the difference in spectral amplitude.

displayed for both texture regions, as well as the spectral differences between these two distributions. It can be seen that spectral differences exist at two distinct off-orientation bands (centered at roughly +30 and -30 degrees). An OM may thus be thought of as two co-occurring counter phase contrast modulations, each within a relatively narrow band of orientations. As a result, any FRF mechanism whose first-order filters are selective to one of the two modulated ranges of orientations would be able to signal this OM.

There are thus two classes of FRF mechanisms that would be able to detect an OM: One class of FRF mechanisms has first-order filters tuned to the counter-clockwise off-orientation band (relative to the texture's average orientation), the other has first-order filters tuned to the clockwise off-orientation band. However, since either class of FRF mechanism signals contrast differences only in the channel for which its first-order filters are selective, neither mechanism alone can signal the nature of the modulation. For example, it is not hard to see that an OM whose texture regions are centered around orientations 50 and 70 degrees will have a contrast modulation in the off-orientation band centered on about 30 degrees (as the OM in Fig. 1 does), but now coupled with a contrast-modulation in an orientation band centered around 90 degrees. Thus, activity in an FRF mechanism with first-order filters tuned to 30 degrees could arise from an OM centered around 0 degrees (horizontal) or from an OM centered around 60 degrees. Indeed, contrast modulations within any given orientation/spatial frequency band may arise from an OM, a contrast-modulation (CM), frequency-modulation (FM) or any combination thereof. Thus, in order merely to *detect* a texture modulation it would suffice to detect a contrast modulation in a single orientation/spatial frequency channel, but in order to *identify* the nature of the modulation, contrast modulations need to be detected in two orientation/spatial frequency channels. One would expect, then, that detection performance would be superior to identification performance. Prins and Kingdom (2003), however, have shown that detection and identification thresholds are approximately equal. This suggests that FRF mechanisms with different first-order selectivity may interact.

Two previous studies have addressed this issue directly with contrasting results. Motoyoshi and Nishida (2004) presented participants with textures consisting of two transparent texture planes, one containing micropatterns oriented at 45°, the other containing micropatterns oriented at -45°. Participants were to detect the location of a texture region defined by a difference in contrast of the micropatterns in either or both of the texture planes. Their results indicated that participants acted solely on overall contrast. That is, modulation amplitudes added in a linear fashion to determine performance. Based on this result, Motoyoshi and Nishida concluded that, for this stimulus, first-order contrast is

pooled across orientation before second-order integration is performed. Such pooling may occur either by integrating the rectified output of all first-order filters (regardless of their orientation tuning) or by integrating the rectified output of first-order filters which themselves are not selective for orientation.

On the other hand, in an extensive series of experiments, Graham and Wolfson (2004) investigated whether modulations in two orthogonal orientations are integrated by a single FRF mechanism or, alternatively, detected by two independent FRF mechanisms. Their results were consistent with what I will refer to here as the 'standard FRF model' (i.e., one in which the first-stage filters are selective for a narrow range of orientations and spatial frequencies) in that modulations in two orthogonal orientations were as detectable, approximately, as the most detectable modulation in the two orientations.

In the current paper, Experiment 1 addresses this issue in a relatively natural context, namely that of an orientation-modulated (OM) texture. The question addressed in Experiment 1 is whether an OM's deviations from an unmodulated texture are detected independently or interact. Consider again the OM texture in Fig. 1. This texture differs in four respects from an unmodulated texture of the same average orientation. Relative to the unmodulated texture, the regions labeled 1 in the Figure contain more energy in an off-orientation band clockwise from horizontal and less energy in an off-orientation counterclockwise from horizontal. The opposite is true of regions labeled 2. In Experiment 1, textures are created in which these deviations from an unmodulated texture are manipulated independently. For example, both textures in Fig. 2 were created by adding contrast energy in two off-orientation bands to an unmodulated texture which was centered on the horizontal orientation. In the texture in Fig. 2a, the contrast energy in both bands was added to identical texture regions (those labeled 1). In the texture in Fig. 2b, contrast energy in the counter-clockwise off-orientation was added to texture regions labeled 1, whereas contrast energy in the clockwise off-orientation band was added to regions labeled 2. In other words, both textures now contain contrast modulations in two distinct orientation channels, but whereas in the first texture these contrast modulations are in-phase, in the second texture they are counter-phase.

If these two within-channel contrast modulations are detected independently, the texture bars in Fig. 2a and b should be equally detectable, despite their different appearance. This would be expected in case the modulations are detected by the standard FRF mechanisms described above. Given that the two modulations occur in distinct orientation channels, they would be detected by separate FRF mechanisms. Assuming these FRF mechanisms operate independently, the probability of detection of either modula-

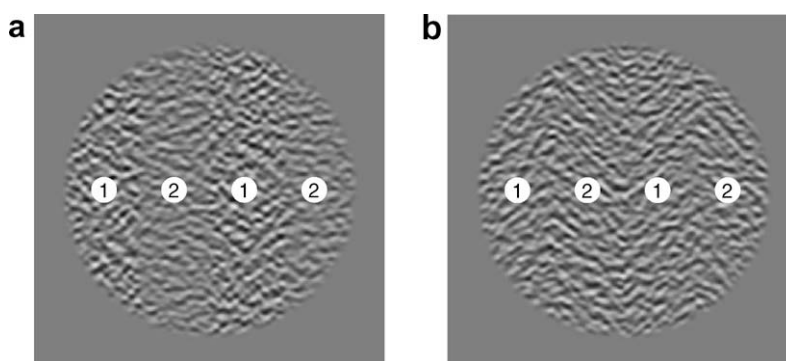


**Fig. 2.** Both textures here were created by adding contrast energy in two off-orientation (relative to horizontal, the average orientation) channels to an unmodulated texture. (a) energy in both channels is added to identical texture regions (those labeled 1). (b) energy in the counter-clockwise off-orientation channel is added to regions labeled 1 and energy in the clockwise off-orientation channels is added to regions labeled 2. As a result, the texture in (a) contains a modulation in overall contrast but no modulation in average orientation. The reverse is true for the texture in (b).

tion would be determined by probability summation between the two classes of FRF mechanisms.

Interactions between channel modulations may occur in several manners. A mechanism which acts on the overall contrast in the texture regions (e.g., Motoyoshi & Kingdom, 2007; Motoyoshi & Nishida, 2004) would detect modulations in overall contrast. Such a mechanism may be able to detect the texture modulation in Fig. 2a, where the contributions of the two within-channel contrast modulations combine to result in a modulation of overall contrast. Such a mechanism would, however, not be able to detect the modulation in Fig. 2b since the two within-channel contrast modulations are in counter-phase and no modulation of overall contrast results. On the other hand, any mechanism that compares some single abstracted measure of orientation (e.g., mean orientation) between texture regions would have a lower threshold for the texture in Fig. 2b (since the two contrast modulations are combined in such a manner that the mean orientations in the texture regions are shifted in opposite directions) but would not be able to detect the modulation in the texture in Fig. 2a (since the contrast modulations are combined in such a manner that no shift in mean orientation results). The latter type of mechanism has been proposed by some versions of feature models (e.g., Treisman, 1985).

## 2. Experiment 1

All textures utilized in Experiment 1 were created by modulating the contrasts in two narrow orientation bands in an orientationally broadband texture. The modulation of contrast in the two orientation bands followed a square-wave pattern across the texture thereby defining alternating bars. The task of the observers was to determine whether these bars were oriented 45 degrees to the left or right of vertical.

### 2.1. General methods

#### 2.1.1. Stimuli

Textures consisted of a multitude of micropatterns distributed across a circular stimulus area (radius = 3 degrees). Micropatterns were created by defining their spectral content in the Fourier domain. Defining micropatterns in Fourier space allows for flexible and precise control over the spectral content of the texture regions. All micropatterns were designed to contain a 'base' distribution of energy across a limited range of orientations and spatial frequencies. Modulations were then created by adding or subtracting energy in off-orientation sidebands to or from the base distribution.

Amplitude spectra are thus considered to consist of three components: one base component as well as two sideband components ( $C_1$  and  $C_2$ ). A graphical representation of amplitude across orientation for these three components is shown in Fig. 3. The base distribution of spectral amplitude as a function of spatial frequency ( $f$ , in cpd) and orientation ( $\theta$ , in degrees) was defined by:

tation for these three components is shown in Fig. 3. The base distribution of spectral amplitude as a function of spatial frequency ( $f$ , in cpd) and orientation ( $\theta$ , in degrees) was defined by:

$$L_{\text{base}}(f, \theta) = F(f)O_{\text{base}}(\theta), \text{ where} \quad (1a)$$

$$F(f) = 0.5 + 0.5 \cos\left(\pi \frac{\log_2(f/f_0)}{bw_f}\right), f_0 \times 2^{-bw_f} < f < f_0 \times 2^{bw_f} \quad (1b)$$

$$F(f) = 0, \text{ elsewhere}$$

$$O_{\text{base}}(\theta) = 0.5 + 0.5 \cos\left(\pi \frac{\theta - \theta_0}{bw_\theta}\right), \theta_0 - bw_\theta < \theta < \theta_0 + bw_\theta \quad (1c)$$

$$O_{\text{base}}(\theta) = 0 \text{ elsewhere.}$$

where peak frequency  $f_0 = 3.5$  cpd, frequency bandwidth (full-width at half-height)  $bw_f = 1.5$  (octaves), peak orientation  $\theta_0 = 0^\circ$  (horizontal), and orientation bandwidth  $bw_\theta = 90^\circ$ .

The spectral distributions of the sideband components were defined by:

$$L_{C_1}(f, \theta) = F(f)O_{C_1}(\theta), \quad (2a)$$

and

$$L_{C_2}(f, \theta) = F(f)O_{C_2}(\theta) \quad (2b)$$

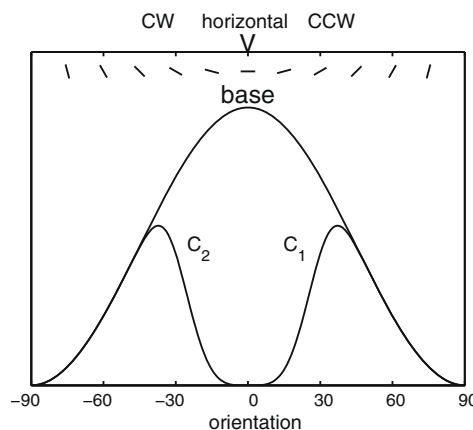


**Fig. 3.** Spectral distributions (across orientation only) of the base texture and sideband components used to create the textures in Experiment 1. The base texture is centered on  $0^\circ$  (horizontal). Sideband component 1 ( $C_1$ ) is centered on an orientation counterclockwise relative to horizontal. Sideband component 2 ( $C_2$ ) is centered on an orientation clockwise relative to horizontal.

where

$$O_{C_1}(\theta) = \left(0.5 + 0.5 \cos\left(\pi \frac{\theta - \theta_0}{bw_\theta}\right)\right) \times \left(1 - e^{-1 \times \left(\frac{\theta - \theta_0}{30}\right)^4}\right),$$

$$0 < \theta < \theta_0 + bw_\theta \quad (2c)$$

$O_{C_1}(\theta) = 0$ , else where and

$$O_{C_2}(\theta) = \left(0.5 + 0.5 \cos\left(\pi \frac{\theta - \theta_0}{bw_\theta}\right)\right) \times \left(1 - e^{-1 \times \left(\frac{\theta - \theta_0}{30}\right)^4}\right),$$

$$\theta_0 - bw_\theta < \theta < 0 \quad (2d)$$

$O_{C_2}(\theta) = 0$ , elsewhere.

$F(f)$ ,  $\theta_0$ ,  $bw_e$  are as defined above. The peak amplitude of the sidebands lies at 37 degrees from horizontal.

The phase spectrum was defined to be uniform at 0°, resulting in even-symmetric, cosine-phase micropatterns. Anti-cosine micropatterns were also created, simply by inverting the polarity of the cosine-phase micropatterns. Note that since the spectral amplitude at frequency  $f = 0$  was defined to equal 0, micropatterns as created are dc-balanced. This ensures that texture regions were of same average luminance as the background. The spectral distributions were defined on a  $41 \times 41$  pixel ( $1.13 \times 1.13$  degrees) grid, which is the same resolution as was used for the micropatterns themselves. The size of the micropattern grid was sufficiently large to avoid, effectively, any cropping effects. All figures showing examples of textures used in the experiments also contain images of the micropatterns that were used to create the textures (these micropatterns were of course not shown during experimental testing). The icons in the figures schematically indicate the texture bars which contain the two micropatterns shown to the right of the icons.

Fig. 4 shows example texture regions corresponding to the base ('base'), base + counterclockwise (CCW) sideband component ('C<sub>1</sub>+'), base – CCW sideband component ('C<sub>1</sub>-'), base + CCW sideband component + CW sideband component ('C<sub>1</sub>+C<sub>2</sub>+'), and base – CCW sideband component – CW sideband component ('C<sub>1</sub>-C<sub>2</sub>-'). CW and CCW are defined relative to horizontal, the peak orientation in the base texture. The mirror images of the texture regions

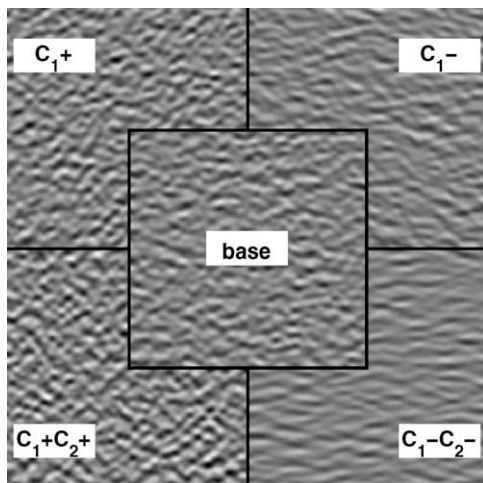


**Fig. 4.** Example texture regions consisting of different combinations of the base texture and off-orientation components. The center square ('base') was created from micropatterns whose amplitude spectra corresponded to that of 'base' (Fig. 3). Other regions were created from micropatterns whose amplitude spectra were a combination of that of 'base' and sideband component 1 ( $C_1$ ) and/or 2 ( $C_2$ ). Note that contrast and average orientation vary in a predictable manner. For example, the top left texture region was created by adding energy in a counterclockwise sideband ( $C_1$ ) to 'base' (hence the label 'C<sub>1</sub>+'). As a result, the texture has higher contrast and the average orientation has shifted in the counterclockwise direction. Note also that the mirror images of  $C_1+$  and  $C_1-$ , would be  $C_2+$  and  $C_2-$ , respectively.

in Fig. 4 would be, respectively, 'base', 'C<sub>2</sub>+', 'C<sub>2</sub>- ', 'C<sub>1</sub>+C<sub>2</sub>+', and 'C<sub>1</sub>-C<sub>2</sub>- '. From the figure we note again that, depending on the combination of components added to/subtracted from the base, the perceived overall orientation of the texture and the overall contrast of the texture changes in predictable ways.

The textures used in the experiment were square-wave modulated by dividing the texture into alternating bars and distributing micropatterns such that the centers of micropatterns created from the two different combinations of base,  $C_1$  and  $C_2$  were located in alternate texture bars. The wavelength of the square-wave modulation was equal to the radius of the stimulus area (3 degrees), the phase of the modulation was selected randomly (from a uniform probability density function spanning 360°) and the orientation of the texture bars was either +45 or –45 degrees.

Micropatterns were distributed randomly across the texture. A few constraints on placement were applied. First, the center of micropatterns was constrained to fall within the circular texture area. Second, the center of micropatterns with differing Fourier amplitude spectra were constrained to lie within the alternating texture bars. Since micropatterns whose center was near a border between texture bars extend into the neighboring bar and overlap with micropatterns centered in the neighboring bar, a smooth transition between the texture bars resulted. The final constraint on placement was that the minimum distance between the centers of any two micropatterns was at least 6.6 min. This constraint ensured approximately equal coverage across the texture area while also avoiding excessive luminance overlap and the need for 'luminance clipping'. Where micropatterns overlapped, their contrasts were added. The density of micropatterns across the texture area was 57.2 micropatterns/degree<sup>2</sup>. The number of micropatterns of each kind was determined for every texture individually since the relative areas of the alternating texture regions varied from trial to trial with the phase of the modulation. Within each of the two different texture areas an equal number of cosine and anti-cosine phase micropatterns was used. After the micropatterns were distributed across the texture region, the perimeter of the texture was smoothed by a contrast ramp.

In three different conditions, the distribution of contrast energy between alternating texture bars was varied in different manners. In the first condition, textures were created by alternating bars containing the base texture only and bars containing the base texture plus some combination of the two sideband components. For convenience, this condition will be denoted '0|C<sub>1</sub>C<sub>2</sub>'. This notation reflects the distribution of energy across the texture regions: One texture region contains the base only and is denoted '0', the other contains the base plus some combination of sideband components and is denoted 'C<sub>1</sub>C<sub>2</sub>'.

Specifically, the amplitude spectrum of the texture bars consisting of the base only was:

$$L_1 = L_{\text{base}}, \quad (3a)$$

That in the alternate bars was:

$$L_2 = L_{\text{base}} + m_1 \times L_{C_1} + m_2 \times L_{C_2} \quad (3b)$$

where  $L_{\text{base}}$ ,  $L_{C_1}$  and  $L_{C_2}$  are as defined in Eqs. (1) and (2), and  $m_1$  and  $m_2$  were varied as:

$$m_1 = A \times \cos(\phi) \quad (3c)$$

$$m_2 = A \times \sin(\phi) \quad (3d)$$

The relative amplitudes of the sideband spectra was varied by varying angle  $\phi$  (Eqs. (3c) and (3d)) from 0° to 337.5° in steps of 22.5°. A determines the amplitude of modulation. Fig. 5 shows the relationship between  $m_1$ ,  $m_2$ ,  $\phi$  and  $A$  graphically. Fig. 6a and b shows example textures in condition 0|C<sub>1</sub>C<sub>2</sub>. In the texture in Fig. 6a, the

value of angle  $\phi$  equals  $45^\circ$  and  $A$  equals  $\sqrt{2}$ , thus  $m_1$  equals +1 and  $m_2$  equals +1 (Eq. (3)). In words, bars containing just the base spectral distribution are alternated with bars in which contrast energy in both the counterclockwise sideband component ( $C_1$ ) and the clockwise sideband component ( $C_2$ ) is added to the base spectrum. Thus the bars differ in overall contrast but the texture is, in all the bars, centered on the horizontal orientation. In the texture in Fig. 6b, the value of angle  $\phi$  equals  $135^\circ$ ,  $A$  again equals  $\sqrt{2}$ , and thus  $m_1$  and  $m_2$  are of opposite sign ( $m_1$  equals -1 and  $m_2$  equals +1). In words, bars containing just the base spectral distribution are alternated with bars in which contrast energy in the counterclockwise sideband component ( $C_1$ ) is added to the base spectrum but contrast energy in the clockwise sideband component ( $C_2$ ) is subtracted from it. Here, the bars are equal in overall contrast but the texture is now orientation modulated in that the average orientation in one of the bars is shifted clockwise. Note that the mirror image of this texture would be equivalent to a texture at angle  $\phi = 315^\circ$ . Some textures at other angles  $\phi$  consist of combinations of texture areas shown in Fig. 4. For example, when angle  $\phi$  equals  $225^\circ$  ( $m_1$  and  $m_2$  are both negative and of equal value), bars containing the base texture are alternated with bars containing the  $C_1$ - $C_2$ - texture. Supplemental Figure S.1a contains example textures at all angles  $\phi$  between  $0^\circ$  and  $315^\circ$  in steps of  $45^\circ$ .

In the second condition, textures were created by alternating bars containing the base texture to which one of the sidebands was added and bars containing the base to which the other sideband was added. Analogous to the notation in the first condition, this condition will be denoted ' $C_1|C_2$ '.

Specifically, the amplitude spectrum of the texture bars were:

$$L_1 = L_{\text{base}} + m_1 \times L_{C_1} \quad (4a)$$

and

$$L_2 = L_{\text{base}} - m_2 \times L_{C_2} \quad (4b)$$

Modulation amplitudes  $m_1$  and  $m_2$  were varied as in Experiment 1a. Fig. 6c shows an example texture where angle  $\phi = 45^\circ$  and  $A = \sqrt{2}$ . In this texture, the sideband components cancel their contributions to a modulation in overall contrast but add their contributions to a modulation in average orientation (the shifts in average orientation of the texture regions are in opposite directions). Supplemental Figure S.1b contains example textures at all angles  $\phi$  between  $0^\circ$  and  $315^\circ$  in steps of  $45^\circ$ .

In the third condition, the distributions of contrast energy in the two texture regions were:

$$L_1 = L_{\text{base}} + m_1 \times L_{C_1} + m_2 \times L_{C_2} \quad (5a)$$

and

$$L_2 = L_{\text{base}} - m_1 \times L_{C_1} - m_2 \times L_{C_2} \quad (5b)$$

Modulation amplitudes  $m_1$  and  $m_2$  were varied as in Experiment 1a. This condition will be denoted  $C_1C_2|C_1C_2$ . Note that when angle  $\phi = 135^\circ$  or  $315^\circ$  (i.e.,  $m_1 = -m_2$  and the two sideband components are thus modulated in counter-phase), the resulting texture is, in effect, an OM such as that shown in Fig. 1. The texture in Fig. 6d is an example  $A = \sqrt{2}$  texture in this condition at  $\phi = 135^\circ$ . When angle  $\phi = 45^\circ$  or  $225^\circ$  (i.e.,  $m_1 = m_2$  and the two sideband components are modulated in phase), the resulting texture contains a modulation of overall contrast but not orientation (the texture in Fig. 6e is an example [ $A = \sqrt{2}$ ]). Supplemental Figure S.1c contains example textures at all angles  $\phi$  between  $0^\circ$  and  $315^\circ$  in steps of  $45^\circ$ . Note that in this condition, a shift in angle  $\phi$  by  $180^\circ$  is equivalent to a shift in second-order phase by  $180^\circ$  (this is most easily realized from Figure S.1c). Since on every trial second-order phase was randomized, angle  $\phi$  and  $\phi + 180^\circ$  are equivalent conditions in condition  $C_1C_2|C_1C_2$ .

### 2.1.2. Procedure

Stimuli were presented on a Mitsubishi Diamondpro 2070SB CRT monitor running at  $800 \times 600$  pixel resolution and 100 Hz refresh rate and driven by a Cambridge Research Systems VSG2/5 graphics board. Background luminance was  $52.8 \text{ cdm}^{-2}$ . RMS contrast of the base texture was 0.146. Viewing distance was 1 m. Stimulus generation, stimulus presentation and response collection were controlled by a custom-written Matlab program. Each trial consisted of the presentation of a texture for 250 ms. The amplitude of modulation ( $A$ , Eq. (3)) was controlled by an adaptive method (the  $\psi$ -method; Kontsevich & Tyler, 1999) for each angle  $\phi$  separately. The  $\psi$ -method chooses stimulus amplitudes on a trial-by-trial basis such as to minimize the expected entropy in the Bayesian posterior likelihood distribution based on previous trials. For each (but the first) block of trials, the prior likelihood used in the  $\psi$ -method was the posterior likelihood obtained from the previous block. In the first block, a uniform prior was used. Micropatterns and textures were generated anew for each trial based on the amplitude dictated by the  $\psi$ -method. After each presentation, observers indicated through a button press whether the texture bars were oriented left diagonally or right diagonally. Feedback was provided in the form of a tone following each response. Trials were run in blocks consisting of 160 trials, 10 trials at each of the 16 values of  $\phi$ , which were randomly interleaved.

NP (author) and four naïve observers (JR, KD, MJM, and WLA) participated in Experiment 1. NP, JR, KD, and WLA participated in all three conditions. MJM participated in condition  $C_1C_2|C_1C_2$  only. All observers tested in at least 18 blocks of 160 trials per condition.

### 2.2. Analysis and model fits

Data were collapsed across the two sideband components. For example, in conditions  $0|C_1C_2$  and  $C_1|C_2$  when angle  $\phi = 0^\circ$ , contrast in sideband 1 is modulated but contrast in sideband 2 is not. The reverse is true at angle  $\phi = 90^\circ$ . In essence, to assume that these conditions are equally detectable is to assume that modulations are equally detectable whether the texture is viewed directly or as its mirror-image. In conditions  $0|C_1C_2$  and  $C_1|C_2$ , there are thus nine resulting combinations of angles ( $\phi = 0^\circ$  and  $90^\circ$ ;  $\phi = 22.5^\circ$  and  $67.5^\circ$ ;  $\phi = 45^\circ$ ;  $\phi = 112.5^\circ$  and  $337.5^\circ$ ;  $\phi = 135^\circ$  and  $315^\circ$ ;  $\phi = 157.5^\circ$  and  $292.5^\circ$ ;  $\phi = 180^\circ$  and  $270^\circ$ ;  $\phi = 202.5^\circ$  and  $247.5^\circ$ ;  $\phi = 225^\circ$ ). In condition  $C_1C_2|C_1C_2$ , results were further collapsed across any angle  $\phi$  and angle  $\phi + 180^\circ$ , since these angles lead to identical textures in this condition (Section 2.1.1). For each of the

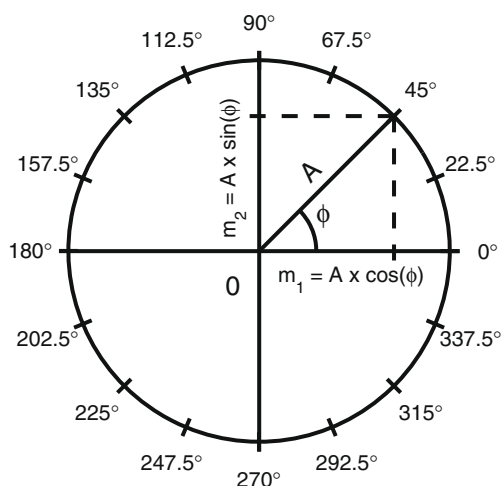
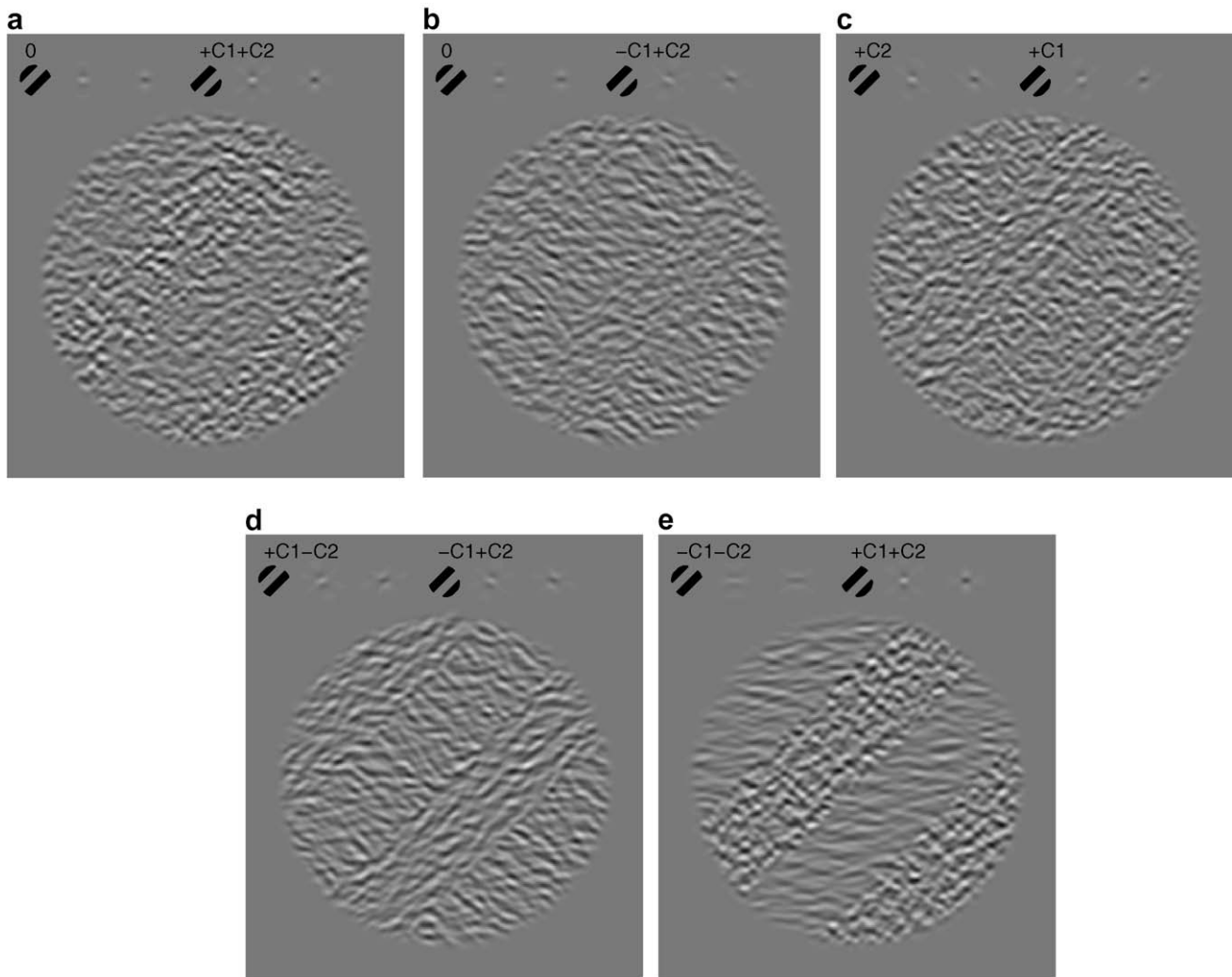


Fig. 5. The relation between  $A$ , angle  $\phi$ ,  $m_1$  and  $m_2$  (Eqs. (3c) and (3d)).



**Fig. 6.** Example textures Experiment 1. (a) condition  $0|C_1C_2$ ,  $\phi = 45^\circ$ ,  $A = \sqrt{2}$ . (b) condition  $0|C_1C_2$ ,  $\phi = 135^\circ$ ,  $A = \sqrt{2}$ . (c) condition  $C_1|C_2$ ,  $\phi = 45^\circ$ ,  $A = \sqrt{2}$ . (d) condition  $C_1C_2|C_1C_2$ ,  $\phi = 135^\circ$ ,  $A = \sqrt{2}$ . (e) condition  $C_1C_2|C_1C_2$ ,  $\phi = 45^\circ$ ,  $A = \sqrt{2}$ . Note that for the purposes of illustration, all texture phases are identical and fixed such that bar edges coincide with texture edges. During the experimental trials, the phase of each texture was shifted randomly. Also note that the micropatterns which make up the texture are shown. The icons schematically indicate the texture bars which contain the two micropatterns to the right of the icons. The two micropatterns in each pair are identical save for a reversal in polarity. Also shown with icons are the components which make up the texture bars ('0' base only, '+C1' component 1 added to base, etc.). More example textures are shown in [Supplemental materials](#).

resulting combinations, thresholds and slopes were estimated by fitting Weibull functions relating proportion correct to modulation amplitude  $A$  using a maximum likelihood criterion. The guess rate was assumed to equal 0.5 and the lapse rate was assumed to be 0. The thresholds thus correspond to (approximately) 82% correct performance. Standard errors were found by Bootstrap analysis ( $B = 400$ ; Efron & Tibshirani, 1993).

However, as the contrast in the sidebands was added to that of the base, there is no simple relation between  $A$  (and  $m_1, m_2$ ) on the one hand and overall contrast or contrast within any particular orientation channel on the other hand. In order to plot these thresholds in terms of some metric which would reasonably correspond to the signal available to relevant standard FRF channels, some assumptions were made regarding the first-order filter properties of such mechanisms. For the purposes of modeling the responses in terms of probability summation among two standard FRF mechanisms and an isotropic FRF mechanism we also need to transform modulation amplitudes  $A$  into a metric appropriate for an isotropic FRF mechanisms.

Modulation amplitudes were transformed as follows. Consider Fig. 7. Panel A shows the amplitude spectra across orientation for

two alternate regions of a texture. These spectra correspond to the two texture regions in a texture at the threshold amplitude for observer KD at angles  $\phi = 135^\circ$  and  $315^\circ$  (the example shows spectra at  $\phi = 135^\circ$ ) in condition  $0|C_1C_2$ . KD's threshold in this condition was  $A = 0.704$ . Thus,  $m_1 = 0.704 \times \cos(135^\circ) = -0.498$  (Eq. (3c)) and  $m_2 = 0.704 \times \sin(135^\circ) = 0.498$  (Eq. (3d)). The solid line corresponds to the spectrum in some of the texture bars:  $L_1 = L_{\text{base}}$  (Eq. (3a)), the broken line corresponds to the spectrum in the alternate texture bars:  $L_2 = L_{\text{base}} + (-0.498) \times L_{C_1} + (0.498) \times L_{C_2}$  (Eq. (3b)).

Here, the filter response of an isotropic linear filter to a micropattern is proportional to the integral of the spectral amplitude of that micropattern evaluated across all orientations. Since we are interested in relative responses only, we define the integral for the base texture to equal 1, for convenience. The integral for the alternate texture region would then equal 1 as well, since the integral has the same value for both spectra. Modulation amplitude will be quantified here as Michelson contrast on the values of the integral which in this case would equal  $M_{\text{iso}} = (1 - 1)/(1 + 1) = 0$ , where the subscript 'iso' indicates that this measure refers to the amplitude of modulation considered across all orientations.

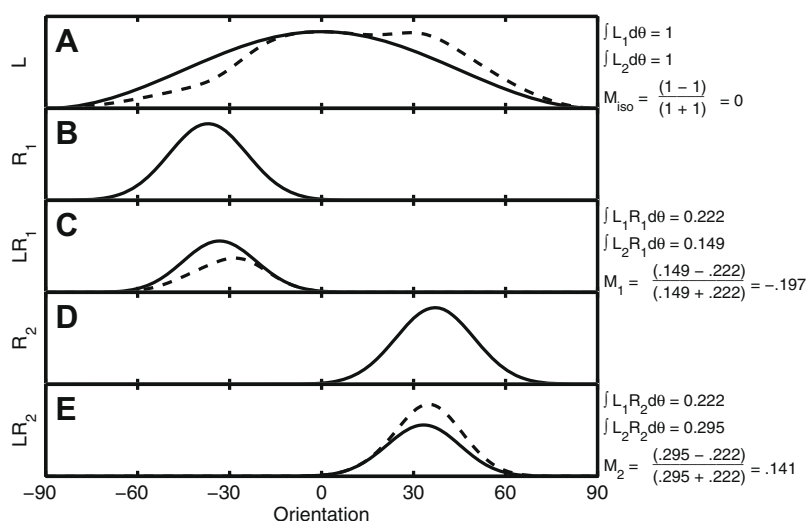


**Fig. 7.** Transformation of modulation amplitudes  $m_1$  and  $m_2$  into modulation amplitude metrics relevant to standard FRF mechanisms and an isotropic FRF mechanism. Modulation amplitude relevant to an isotropic mechanism was expressed in terms of Michelson contrast on the integrals of the spectra of the texture regions across all orientations (Panel A). Modulation amplitudes relevant to standard FRF mechanisms was expressed in terms of Michelson contrast on the value of the integrals of spectra after filtering by relevant first order filters. The response profiles of these filters are modeled as shown in panels (B) and (D), contrast of the texture regions within these channels are shown in panels C and E, respectively. See text for more details.

Standard FRF mechanisms, however, integrate responses of first-order filters which are selective for narrow orientation channels. In order to quantify modulation amplitude within orientation channels which would correspond to the first-order stage of standard FRF mechanisms, the following considerations were made. First, it was assumed that the orientation tuning function of the first-order filters of FRF mechanisms is described by a Gaussian distribution and has an orientation bandwidth of  $30^\circ$  (full-width at half-height). These choices seem reasonable given what is known regarding the response properties of simple cells (e.g., DeValois & DeValois, 1988). Moreover, within a quite wide range of values the exact choice of the bandwidth does not appreciably affect the pattern of results or the goodness-of-fit of models. Second, it was assumed that the first-order orientation filters would be centered on the peak orientations in the modulated sidebands (i.e.,  $37^\circ$  clockwise or counterclockwise relative to horizontal). The exact choice of the location of filters in orientation space is also not critical to the pattern of results or goodness-of-fit of models.

Panel B shows the response function of such a channel centered on sideband 1 ( $R_1$ ). Panel C shows the cross-product of the spectra of the texture regions ( $L_1$  and  $L_2$ ) with that of the channel response ( $R_1$ ). One may think of these as the spectra of the texture regions after filtering with a filter with response function  $R_1$ . The filter response of the filter with the orientation response  $R_1$  to the texture regions will again be proportional to the integrals of the spectra across orientation. The values of these integrals are given in the Figure (both values are relative to the full spectra in A). It is assumed that the Weber ratio is the appropriate metric and thus we define our measure as Michelson on the filter responses within this channel ( $M_1 = -0.197$ ). This is given a negative value merely to indicate that the contrast modulation was implemented by a decrease in contrast relative to the base texture. Panel D and E are analogous to Panels B and C but now with respect to the first-order channel centered on sideband 2. Note that, in spite of  $m_1$  and  $m_2$  having equal (absolute) values,  $M_2 (=0.141)$  does not correspond in absolute value to  $M_1$ . Note also that, being based on relative activations, none of the values of  $M_1$ ,  $M_2$ , and  $M_{iso}$  would be affected by the particular frequency response of the first-order filters such that we do not need to make assumptions regarding the frequency response of the first-order filters. That is, the values of all the filter responses (i.e., the integrals in Fig. 7) would be affected by the

same factor by changes in the frequency response of the first-order filter and the Michelson ratio would consequently be unaffected.

The results were fit under two models which will be referred to as the *two-mechanism model* and the *three-mechanism model*. In the two-mechanism model, performance was assumed to be mediated by probability summation among two standard FRF mechanisms with first-order tuning functions as described above ( $R_1$  and  $R_2$ , Section 2.2 and Fig. 7). This model contained only two free parameters: a (common) threshold and (common) slope parameter for the two standard FRF mechanisms. Details are as described in the Appendix but, in short, the entire set of responses for each observer were fit simultaneously using a maximum likelihood criterion and assuming that performance was mediated by probability summation among two standard FRF mechanisms, one with first-order tuning function as  $R_1$ , the other with first-order tuning as  $R_2$ . Estimates of the threshold and slope parameters of the standard FRF mechanism are displayed in Table 1.

In the three-mechanism model, performance was assumed to be mediated by probability summation among three mechanisms: two standard FRF mechanisms and an isotropic FRF mechanism. The fitting procedure was analogous to that of the model described above, except that the isotropic mechanism was included as well (details are provided in the Appendix). This model contained four free parameters: a (common) threshold and (common) slope parameter for the two standard FRF mechanisms as well as a threshold and a slope parameter for the isotropic mechanism. Threshold predictions under this three-mechanism probability summation model are shown in Fig. 8 by the curved lines. Parameter estimates are displayed in Table 1.

The goodness-of-fit of both models was determined by comparing their fit against that of the 'saturated' model. The saturated model makes no assumptions whatsoever with respect to the shape of the function which relates proportion correct to modulation amplitude or with respect to the manner in which information from the two sideband components are combined. Rather, the saturated model estimates the probability of a correct response for each unique combination of angle  $\phi$  and modulation amplitude A. A variation of the likelihood ratio test (e.g., Hoel, Port, & Stone, 1971) was used. Specifically, the Deviance statistic for both models was calculated on the data of the human observers and compared against sampling distributions created by Monte Carlo simulations

**Table 1**  
Parameter estimates of the two-mechanism probability summation model and the three-mechanism probability summation model for all observers in the three conditions of Experiment 1

	2-Mechanism		3-Mechanism			
	$\alpha_{st}$	$\beta_{st}$	$\alpha_{st}$	$\beta_{st}$	$\alpha_{iso}$	$\beta_{iso}$
NP 0 C <sub>1</sub> C <sub>2</sub>	.142	2.17	.152	2.16	.092	3.77
NP C <sub>1</sub>  C <sub>2</sub>	.129	2.13	.135	2.13	.111	2.77
NP C <sub>1</sub> C <sub>2</sub>  C <sub>1</sub> C <sub>2</sub>	.127	2.26	.130	2.23	.108	4.10
JR 0 C <sub>1</sub> C <sub>2</sub>	.159	1.81	.169	1.80	.151	2.23
JR C <sub>1</sub>  C <sub>2</sub>	.152	2.20	.164	2.28	.127	1.94
JR C <sub>1</sub> C <sub>2</sub>  C <sub>1</sub> C <sub>2</sub>	.216	1.35	.235	1.34	.302	1.45
KD 0 C <sub>1</sub> C <sub>2</sub>	.184	1.69	.221	2.53	.077	2.16
KD C <sub>1</sub>  C <sub>2</sub>	.175	1.81	.209	2.01	.086	2.41
KD C <sub>1</sub> C <sub>2</sub>  C <sub>1</sub> C <sub>2</sub>	.156	2.02	.185	3.17	.066	1.92
MJM C <sub>1</sub> C <sub>2</sub>  C <sub>1</sub> C <sub>2</sub>	.215	2.24	.231	2.32	.164	2.32
WLA 0 C <sub>1</sub> C <sub>2</sub>	xx	xx	xx	xx	xx	xx
WLA C <sub>1</sub>  C <sub>2</sub>	xx	xx	xx	xx	xx	xx
WLA C <sub>1</sub> C <sub>2</sub>  C <sub>1</sub> C <sub>2</sub>	.427	1.50	0.524	1.61	.257	1.52

Failed fits are indicated by 'xx' as parameter estimates (see text for details). (Note that WLA did participate in all three conditions, but models could not be fit successfully in conditions 0|C<sub>1</sub>C<sub>2</sub> and C<sub>1</sub>|C<sub>2</sub>. Observer M.J.M. did not participate in these conditions).  $\alpha_{st}$  and  $\beta_{st}$  are the estimated threshold and slope of the standard FRF mechanisms, respectively.  $\alpha_{iso}$  and  $\beta_{iso}$  are the estimated threshold and slope of the isotropic mechanism.

(e.g., Wichmann & Hill, 2001). Details are provided in the Appendix. All figures contain p-values associated with the statistical comparison between the two-mechanism model and the saturated model ( $p_2$ ) and with the statistical comparison between the three-mechanism model and the saturated model ( $p_3$ ).

2.3. Results and discussion

Thresholds and standard errors were expressed in terms of  $M_1$  and  $M_2$  as outlined above and are plotted as such in Fig. 8a, b, and c for conditions 0|C<sub>1</sub>C<sub>2</sub>, C<sub>1</sub>|C<sub>2</sub>, and C<sub>1</sub>C<sub>2</sub>|C<sub>1</sub>C<sub>2</sub>, respectively. Note that axes are labeled  $M_{channel}$  and  $M_{alternate\ channel}$  (rather than  $M_1$  and  $M_2$ ) to reflect the combination of results across the two sideband orientations. Where standard error bars are not visible, they do not extend beyond the plotting symbol. WLA's thresholds in conditions 0|C<sub>1</sub>C<sub>2</sub> and C<sub>1</sub>|C<sub>2</sub> could not be determined as thresholds were beyond the physical limitations set on A. The amplitude of modulation of overall contrast (based on which an isotropic FRF mechanism would respond) varies with angle  $\phi$  and is not directly represented in the graphs. However, in conditions 0|C<sub>1</sub>C<sub>2</sub> (Fig. 8a) and C<sub>1</sub>C<sub>2</sub>|C<sub>1</sub>C<sub>2</sub> (Fig. 8c) the sideband component contrast modulations add their contributions to a modulation in overall contrast in quadrants 1 and 3, whereas in quadrants 2 and 4 their contributions to an overall contrast modulation cancel. In condition C<sub>1</sub>|C<sub>2</sub> the reverse is true.

Fig. 8a displays the results in condition 0|C<sub>1</sub>C<sub>2</sub>. As the effect of modulation of overall contrast is most pronounced in the results of KD, let us first consider KD's results. First compare the results at angles  $\phi = 45^\circ$  and  $\phi = 135^\circ$ . Fig. 6a and b are example textures at these respective angles. At angle  $\phi = 135^\circ$  (Fig. 6b), energy in one of the sideband components is added to the base spectrum while energy in the other sideband is subtracted from it in an equal amount (i.e.,  $m_1 = -m_2$ ). Both modifications are applied to the same texture bars. The alternate texture bars contain the base texture only. Thus, contributions to an overall contrast modulation cancel and there would be no signal to detect by an isotropic FRF mechanism (i.e.,  $M_{iso} = 0$ ). At angle  $\phi = 45^\circ$  (Fig. 6a), on the other hand, sideband components are both added to the same texture bars and a modulation of overall contrast results. It is clear that, for KD at least, thresholds are much lower at angle  $\phi = 45^\circ$  compared to  $\phi = 135^\circ$ . In general, KD's thresholds are much lower in quadrants 1 and 3 compared to those in quadrants 2 and 4. This re-

sult can not be explained by a model which considers modulation amplitudes in terms of  $M_1$  and  $M_2$  only, or by a model which also incorporates a filter centered on the base texture orientation. However, the pattern of results is readily explained by a model which incorporates an isotropic FRF mechanism. At angle  $\phi = 45^\circ$ , where the texture contains a modulation of overall contrast, such a mechanism would contribute to task performance. At angle  $\phi = 135^\circ$ , however, the texture does not contain a modulation of overall contrast and an isotropic mechanism would not be able to detect the modulation.

In the results of NP and JR, on the other hand, thresholds are approximately equal in all quadrants and there is not much evidence to conclude that an isotropic mechanism was involved in this condition. Indeed, the goodness-of-fit of the two-mechanism model indicates that probability summation among only two standard FRF mechanisms suffices to explain the data.

There is an asymmetry in the results which deserves some discussion. The pattern of thresholds lacks symmetry with respect to the left diagonal. This asymmetry actually confirms the involvement of an isotropic FRF mechanism (as will be discussed), and as one might therefore expect, it is especially apparent in the results of KD. Let us compare the threshold at angle  $\phi = 90^\circ$  ('12 o'clock') to that at angle  $\phi = 270^\circ$  ('6 o'clock'). At both angles, only one of the two sidebands is modulated. However, whereas at angle  $\phi = 90^\circ$  the sideband component is added to the base spectrum, at angle  $\phi = 270^\circ$  the component is subtracted from the base spectrum. When the component is added to the base the plotted threshold is  $M_{channel} = 0.151$ , but when the component is subtracted from the base the threshold is  $M_{channel} = 0.182$  (remember that  $M_{channel}$  is the modeled signal available to a standard FRF mechanism and that the negative sign of M merely indicates that the signal was implemented by subtracting the sideband component from the base). Thus we have an apparent contradiction: Textures at these two thresholds are equally detectable (they are both at threshold) yet they are not equally detectable to standard FRF mechanisms. The apparent contradiction is easily solved if we allow an isotropic mechanism which acts on a modulation amplitude other than  $M_{channel}$  to contribute. The signal available to an isotropic mechanism ( $M_{iso}$ ) does not scale linearly with the signal available to a standard FRF mechanism which is plotted in Fig. 8 ( $M_{channel}$ ). This is demonstrated for the above case in the Appendix (Section A.3). The reasoning there can be easily generalized to other angles.

In condition C<sub>1</sub>|C<sub>2</sub> (Fig. 8b), sideband components combine their contributions to form a modulation of overall contrast in quadrants 2 and 4, whereas in quadrants 1 and 3 contributions are (wholly or partially) canceled. Again we see that an isotropic mechanism appears to play a dominant role in KD's results, but not in the results of NP and JR.

In condition C<sub>1</sub>C<sub>2</sub>|C<sub>1</sub>C<sub>2</sub> (Fig. 8c), sideband components add their contrasts in quadrants 1 and 3. In quadrants 2 and 4 their contrast modulations cancel. Once again, we see that KD's results are especially affected by whether textures contain a modulation in overall contrast. Visual inspection of WLA's results also suggests a role for an isotropic mechanism (although the goodness-of-fit measures can not be used to support this: neither of the two models fits adequately). However, the results of NP and MJM are fit well without the need for an isotropic mechanism. JR's results are fit well by neither model, but visual inspection of JR's results does not unambiguously reveal a role of an isotropic mechanism.

What might be the explanation of the discrepancy between observers? Perhaps the explanation that springs to mind first is that only KD and WLA's visual systems have isotropic FRF mechanisms available. This seems unlikely (indeed, the results of Experiment 2 will suggest strongly that, under different circumstances, observer NP's visual system also utilizes isotropic FRF mecha-

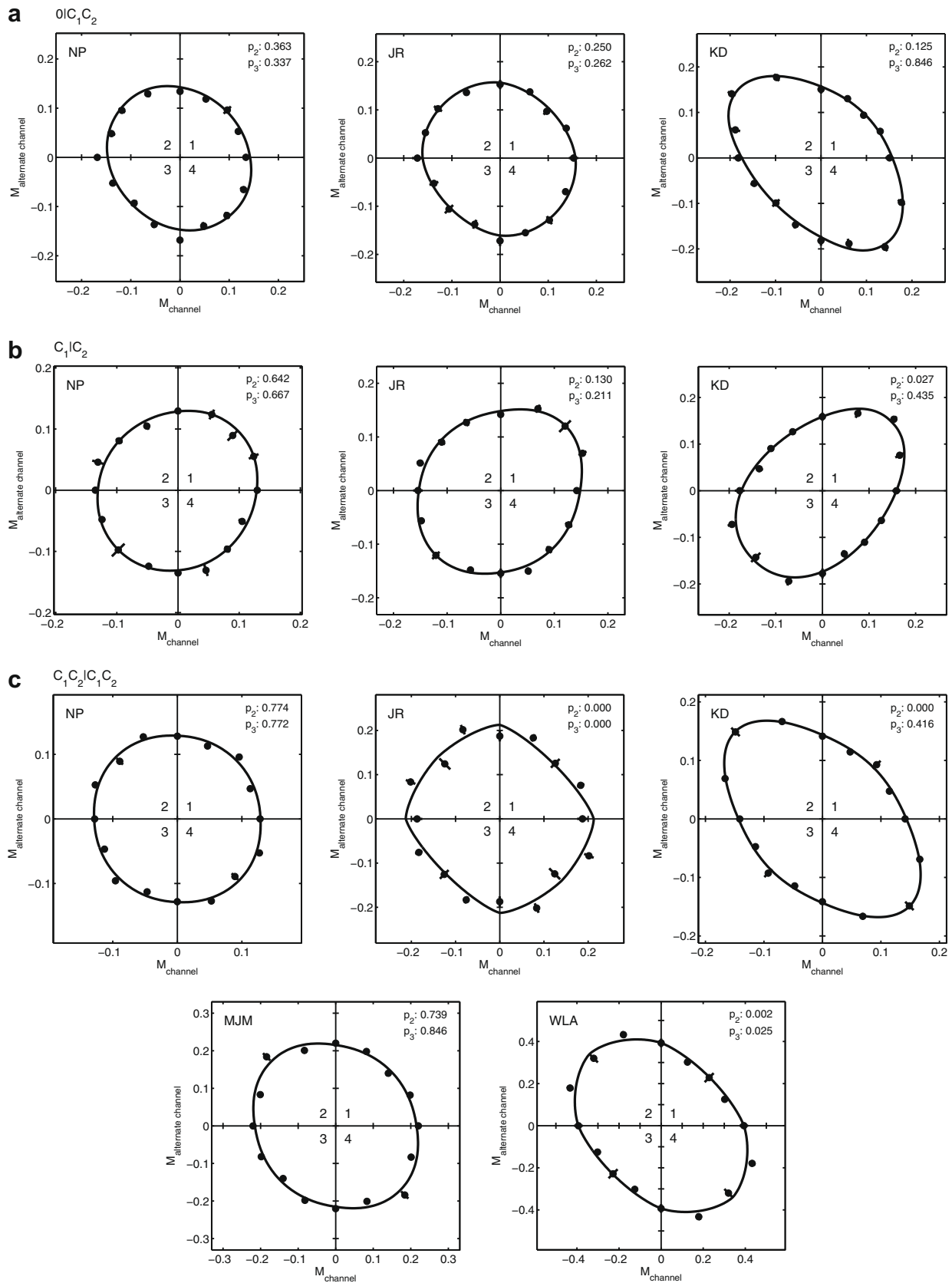


**Fig. 8.** Results of Experiment 1. (a) condition  $0|C_1C_2$  (b) condition  $C_1|C_2$  (c) condition  $C_1C_2|C_1C_2$ . Thresholds are plotted in terms of Michelson on contrast within modeled first-order channels of two standard FRF mechanisms (see Section 2.2). One is tuned to sideband component 1, the other to sideband component 2. As results are collapsed across the two sidebands, all graphs are symmetric around the right diagonal and axes are labeled 'M<sub>channel</sub>' and 'M<sub>alternate channel</sub>' rather than M<sub>1</sub> and M<sub>2</sub>. Note that these graphs are individually scaled as thresholds vary quite a bit among observers. Also shown are fits of a model which assumes that performance is determined by probability summation among three mechanisms: two standard FRF mechanisms and an isotropic FRF mechanism. The  $p_3$  values listed are goodness-of-fit measures of these fits. The  $p_2$  values are goodness-of-fit measures of fits assuming probability summation among two standard FRF mechanisms only.

nisms). A more likely explanation is that the relative efficiencies of standard versus isotropic FRF mechanisms are different between observers. Table 1 shows that whereas the threshold estimates of KD's isotropic mechanism are lower than those of any of the other observers, threshold estimates of KD's standard FRF mechanisms are among the highest when compared to those of the other observers. For the stimuli utilized here, an isotropic mechanism would not be expected to be very efficient. The peak contrast in the textures is at an orientation which is unmodulated (namely the peak orientation in the 'base' spectrum of the texture). By its nature, the isotropic mechanism would collapse across all orientations including those orientations that are not modulated. The efficiency of isotropic mechanisms would thus be affected by the presence of contrast in orientation channels that are irrelevant to the task. The standard FRF mechanisms, on the other hand, are able to 'look' only within narrow orientation bands, thereby excluding contrast in irrelevant orientation bands from second-order analysis. The efficiency of standard FRF mechanisms will thus depend on how well these mechanisms can restrict second-order analysis to the relevant, modulated orientation bands. It is conceivable that the standard FRF mechanisms of KD and WLA are less able to exclude irrelevant orientation bands, making them less efficient compared to the mechanisms of other observers. If so, KD and WLA would rely more heavily on their isotropic FRF mechanisms.

The relative efficiency of standard and isotropic FRF mechanisms can be manipulated within observers by manipulating the presence of contrast in irrelevant (i.e., unmodulated) orientation bands. Whereas standard FRF mechanisms should be affected relatively little by contrast in irrelevant orientation bands, the efficiency of isotropic FRF mechanisms would be affected heavily by the presence of contrast in irrelevant orientation bands. Experiment 2 tests this idea explicitly.

### 3. Experiment 2

Experiment 2 was very similar to Experiment 1 in most respects. The main additional manipulation of interest here is that textures either contained contrast only in orientation bands which are relevant to the task (i.e., bands which are contrast-modulated) or contain contrast in irrelevant orientation bands also. As argued above, the presence of contrast in irrelevant orientation bands would have a relatively minor effect on the efficiency of standard FRF mechanism since such mechanisms, in effect, are able to separate the relevant information from the irrelevant information, by virtue of the relevant and irrelevant information being contained in distinct orientation channels. However, contrast in irrelevant channels would severely affect the efficiency of isotropic FRF mechanisms as such mechanisms are unable to separate relevant from irrelevant channels since they collapse across all orientation channels.

The textures in Experiment 2 contained contrast modulations in two orientation bands centered at orthogonal orientations. The relative modulation amplitude was varied between trials in a manner similar to that in Experiment 1. In Experiment 2a, textures contained contrast only in the modulated orientation bands. In Experiment 2b, the textures also contained contrast in two irrelevant (unmodulated) orientation bands.

#### 3.1. Methods

##### 3.1.1. Stimuli

Textures were created in much the same manner as in Experiment 1. Textures again consisted of multitudes of micropatterns which were designed in Fourier space to contain contrast energy within specific orientation bands. The spectra of the two bands were:

$$L_{C1}(f, \theta) = F(f)O_1(\theta), \text{ and} \tag{6a}$$

$$L_{C2}(f, \theta) = F(f)O_2(\theta) \tag{6b}$$

where the amplitude spectrum across spatial frequency was as in Experiment 1:

$$F(f) = 0.5 + 0.5 \cos\left(\pi \frac{\log_2(f/f_0)}{bw_f}\right), f_0 \times 2^{-bw_f} < f < f_0 \times 2^{bw_f} \tag{6c}$$

$$F(f) = 0, \text{ elsewhere}$$

and the amplitude spectra across orientation were raised cosines:

$$O_j(\theta) = 0.5 + 0.5 \cos\left(\pi \frac{\theta - \theta_0}{bw_\theta}\right), \theta_0 - bw_\theta < \theta < \theta_0 + bw_\theta \tag{6d}$$

$$O_j(\theta) = 0, \text{ elsewhere}$$

where  $\theta_0$  was  $-45^\circ$  (left diagonal) for  $j = 1$  and  $+45^\circ$  (right diagonal) for  $j = 2$  and  $bw_e$  was  $45^\circ$ . A graphical representation of these orientation spectra is provided in Fig. 9. Texture modulations were created by varying contrast in the two orientation bands. The Fourier spectrum in one texture region was:

$$L_1 = (0.5 + m_1) \times L_{C1} + (0.5 + m_2) \times L_{C2} \tag{7a}$$

whereas in the alternate texture regions it was:

$$L_2 = (0.5 - m_1) \times L_{C1} + (0.5 - m_2) \times L_{C2} \tag{7b}$$

$m_1$  and  $m_2$  were defined as:

$$m_1 = A \times \cos(\phi) \tag{7c}$$

$$m_2 = A \times \sin(\phi) \tag{7d}$$

where  $A$  and  $\phi$  were as in Experiment 1 (see also Fig. 5). The second-order structure of the textures (bar-width, texture diameter, etc.) were as in experiment 1.

In Experiment 2a, textures contained energy in the above two orientation bands only. An example texture is shown in Fig. 10a (angle  $\phi = 45^\circ$ , modulation amplitude  $A = 0.4$ ). Example textures at angles  $\phi = 0^\circ, 45^\circ, 90^\circ, 135^\circ$ , and  $180^\circ$  are provided in supplementary Figure S.2a. For the purposes of consistency, this figure actually shows textures at angles  $\phi$  between  $0^\circ$  and  $360^\circ$  (i.e., across all four quadrants). However, save for a phase reversal in the second-order texture bars any angle  $\phi$  is equivalent to angle  $\phi + 180^\circ$  and thus quadrants 3 and 4 essentially repeat quadrants 1 and 2. In Experiment 2b all textures also contained energy in irrelevant orientation bands. The spectra of the irrelevant orientation bands were identical to the relevant orientation bands except that they were shifted in orientation space by  $45^\circ$  (the irrelevant orientation bands are shown in broken lines in Fig. 9). Thus, when modulation amplitude  $A$  was equal to zero the textures were entirely isotropic. Texture modulations were created by varying contrast in the relevant orientation bands  $C_1$  and  $C_2$  as in Experiment 2a while the contrast in the irrelevant orientation bands was held

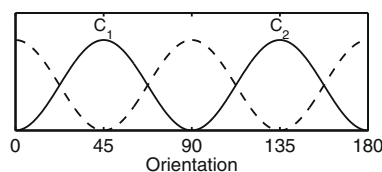
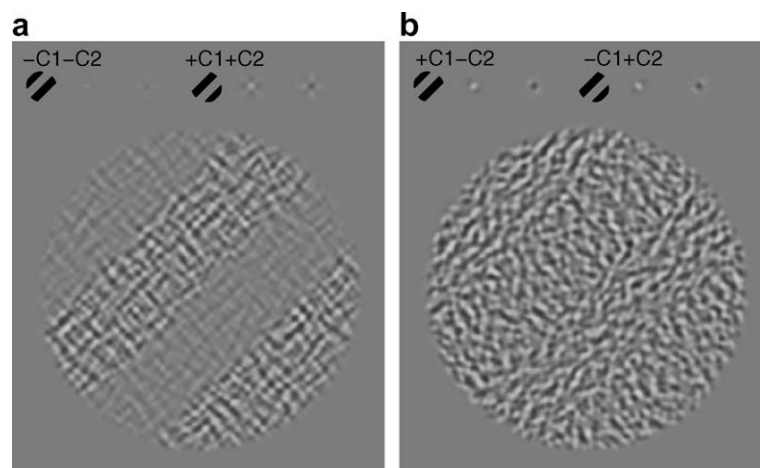


Fig. 9. Amplitude spectra of textures in Experiment 2. In Experiment 2a, textures contained contrast in orientation bands  $C_1$  and  $C_2$  only, which were individually contrast modulated. Textures in Experiment 2b were identical except that they also contained energy contrast energy in irrelevant orientation bands (broken line) neither of which was contrast modulated.



**Fig. 10.** (a) Example texture used in Experiment 2a. Texture contains energy in two bands centered at orthogonal orientations. The contrasts in both bands are modulated at equal amplitude ( $\phi = 45^\circ$ ) and in phase. Modulation amplitude  $A$  (Eq. (7)) equals 0.4. (b) Example texture used in Experiment 2b. The same two bands are contrast modulated at equal amplitude in counter-phase ( $\phi = 135^\circ$ ). Texture also contains contrast in irrelevant orientation channels. Modulation amplitude  $A$  (equation 7) equals 0.4. More example textures are shown in Supplemental materials.

constant. An example texture is shown in Fig. 10b ( $\phi = 135^\circ$ , modulation amplitude  $A = 0.4$ ). Example textures at angles  $\phi = 0^\circ$ ,  $45^\circ$ ,  $90^\circ$ ,  $135^\circ$ , and  $180^\circ$  are provided in supplementary Figures S.2b.

Note that since the orientation of the relevant first-order orientation bands coincide with the orientation of the texture bars, occasional extended carrier contours would form within the texture bars. However, since textures in all conditions contained first-order contrast in orientation bands that were parallel with the texture bars (as well as bands perpendicular to texture bars), the possibility of such extended carrier contours forming existed in all textures regardless of condition, angle  $\phi$ , or orientation of the texture bars. Thus, such cues, insofar as they are used at all, can not act as a confounding variable.

### 3.1.2. Procedure

In separate blocks of trials,  $\phi$  took on either one of the values  $0^\circ$ ,  $22.5^\circ$ ,  $45^\circ$ ,  $67.5^\circ$ , and  $90^\circ$  or one of the values  $90^\circ$ ,  $112.5^\circ$ ,  $135^\circ$ ,  $157.5^\circ$ , and  $180^\circ$ . In the former, when modulations in both bands are present (i.e., at values of angle  $\phi$  other than  $0^\circ$ ,  $90^\circ$ , and  $180^\circ$ ) these contrast modulations are in phase and add to an overall contrast modulation, in the latter they are in counter phase and overall contrast cancels (refer to Fig. 5).

Each block of trials consisted of 200 trials (40 trials at each of the five values of  $\phi$  included in the block). The order of trials within each block was randomized. Modulation amplitude  $A$  was again varied by an adaptive procedure (the ‘ $\psi$ -method’, Kontsevich & Tyler, 1999). Apparatus, viewing distance, presentation duration, etc. were as in Experiment 1. Background luminance was  $52.8 \text{ cdm}^{-2}$ . RMS contrast of unmodulated textures in Experiment 2a was 0.074, in Experiment 2b it was 0.122. The author (NP) and three naïve observers (CBR, ED and KD) tested in Experiment 2. NP and KD also participated in Experiment 1. Each of the participants tested in at least 12 blocks of 200 trials in both Experiment 2a and 2b.

### 3.2. Analysis and model fits

Since no systematic differences were found in performance between the two orientation bands (specifically, between  $\phi = 0^\circ$  and  $\phi = 90^\circ$ , between  $\phi = 22.5^\circ$  and  $\phi = 67.5^\circ$ , between  $\phi = 112.5^\circ$  and  $\phi = 157.5^\circ$ , and between  $\phi = 90^\circ$  and  $\phi = 180^\circ$ ), data were collapsed across these angles. Modulation amplitudes were transformed into

Michelson contrast on modeled mechanism activity in a manner similar to that in Experiment 1 (Section 2.2). The same assumptions were made regarding the presumed first-order filters of the standard FRF mechanisms as in Experiment 1 (i.e., orientation response was Gaussian and had full-width at half-height bandwidth of  $30^\circ$ ). They were assumed to be maximally sensitive to the peak amplitude of the modulated orientation bands (i.e.,  $-45^\circ$  and  $45^\circ$ ). Values for modulation amplitudes in the relevant channels ( $M_1$  and  $M_2$ ) as well as a modulation amplitude relevant to an isotropic mechanism ( $M_{iso}$ ) were then derived as in Experiment 1 (Section 2.2 and Fig. 7).

Derivation of threshold values was as in Experiment 1. Thresholds are plotted in Fig. 11 as a function of  $M_1$  and  $M_2$ . In Fig. 11, the same plotting convention is observed as in condition  $C_1C_2|C_1C_2$  of Experiment 1. That is, thresholds are presented across angles  $\phi$  in the range  $0^\circ$  through  $360^\circ$ , despite the fact that any angle  $\phi$  is equivalent to the angle  $\phi + 180^\circ$  (That is, the data in quadrants 3 and 4 are the same as those in quadrants 1 and 2, respectively). The closed symbols are thresholds obtained in Experiment 2a (in which textures contained energy only in contrast-modulated orientation bands), the open symbols are thresholds obtained in Experiment 2b (in which textures contained energy also in orientation bands which were not contrast-modulated). The size of symbols corresponds to the type of block (in-phase or counter-phase modulation of orientation components) from which the thresholds were derived. Separate thresholds are shown for conditions which were identical but were derived from blocks in which orientation components were modulated in-phase or blocks in which orientation components were modulated in counter-phase. Specifically, angles  $\phi = 0^\circ$  and  $\phi = 90^\circ$  in the in-phase blocks were physically identical to angles  $\phi = 180^\circ$  and  $\phi = 90^\circ$ , respectively, in the counter-phase blocks. At all of these four angles, only one of the orientation bands is modulated and hence the in-phase vs. counter-phase distinction is meaningless at these angles. Thus the only difference between these conditions is the type of block in which they appeared. Any systematic difference between thresholds obtained in these otherwise physically identical conditions could suggest a shift of attention between the different kinds of FRF mechanisms. For example, one might imagine that participants shift attention to the isotropic mechanism in the in-phase blocks compared to the counter-phase blocks. No such systematic difference was observed.

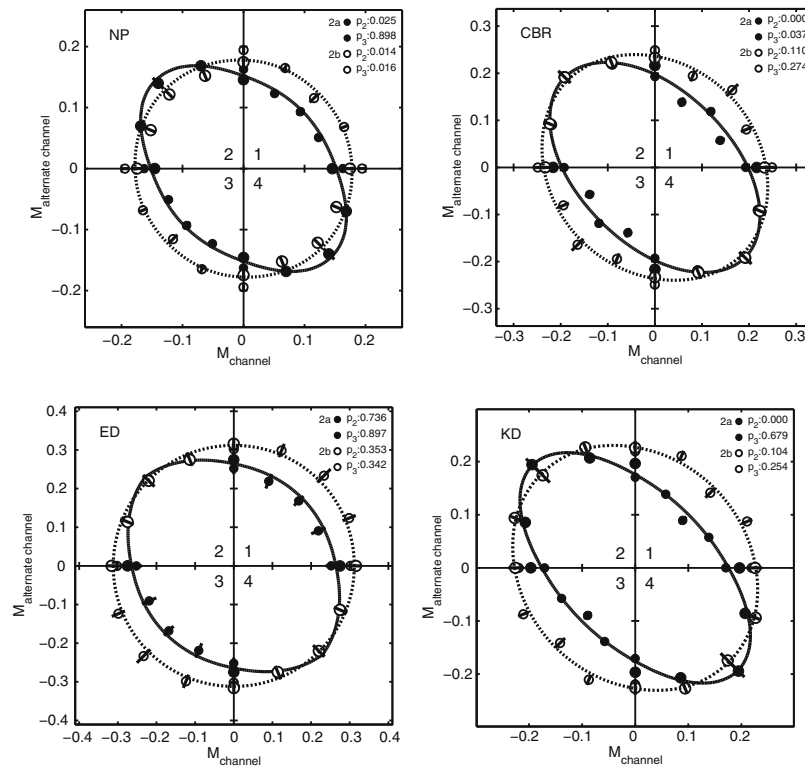


**Fig. 11.** Results of Experiment 2. Closed symbols show thresholds obtained in Experiment 2a, open symbols show thresholds obtained in Experiment 2b. Thresholds are plotted in terms of Michelson on contrast within channels modeled after reasonable first-order channels of two standard FRF mechanisms. One is tuned to sideband component 1, the other to sideband component 2. As results are collapsed across the two sidebands, all graphs are symmetric around the right diagonal and axes are labeled 'M<sub>channel</sub>' and 'M<sub>alternate channel</sub>' rather than M<sub>1</sub> and M<sub>2</sub>. Results are also symmetric with respect to the origin (because texture at any angle  $\phi$  is equivalent with texture at angle  $\phi + 180^\circ$ , see text). Note that these graphs are individually scaled as thresholds vary quite a bit among observers. Also shown are fits of a model which assumes that performance is determined by probability summation among three mechanisms: two standard FRF mechanisms and an isotropic FRF mechanism. The  $p_3$  values listed are goodness-of-fit measures of these fits. The  $p_2$  values are goodness-of-fit measures of fits assuming probability summation among two standard FRF mechanisms only. See text for more details.

The same model fits were performed here as were performed in Experiment 1 (Section 2.3). The fits of the three-mechanism model to the data of Experiment 2a are presented as solid lines in Fig. 11, those to the data of Experiment 2b as broken lines. The estimates of the common threshold and slope for the standard FRF mechanisms ( $\alpha_{st}$ ,  $\beta_{st}$ ) and the threshold and slope estimates for the isotropic FRF mechanism ( $\alpha_{iso}$ ,  $\beta_{iso}$ ) derived under the two-mechanism and three-mechanism model are presented in Table 2 for each of the observers. Goodness-of-fit measures for the two models were determined in the same manner as in Experiment 1 and are presented in Fig. 11 as  $p$  values.

**Table 2**  
Parameter estimates of the two-mechanism probability summation model and the three-mechanism probability summation model for all observers in Experiment 2

Observer	Exp	2-Mechanism		3-Mechanism			
		$\alpha_{st}$	$\beta_{st}$	$\alpha_{st}$	$\beta_{st}$	$\alpha_{iso}$	$\beta_{iso}$
NP	2a	.156	2.32	.184	2.86	.113	2.21
	2b	.174	2.20	.179	2.13	.105	6.88
CBR	2a	.210	1.73	.273	1.94	.146	1.94
	2b	.234	1.97	.260	2.03	.184	1.79
ED	2a	.273	2.03	.312	2.25	.327	1.29
	2b	.312	2.02	.312	2.02	3.68	9.67
KD	2a	.197	1.64	.262	2.28	.114	1.98
	2b	.228	2.06	.247	2.08	.158	2.18

$\alpha_{st}$  and  $\beta_{st}$  are the estimated threshold and slope of the standard FRF mechanisms, respectively.  $\alpha_{iso}$  and  $\beta_{iso}$  are the estimated threshold and slope of the isotropic mechanism.

### 3.3. Results and discussion

The graphs in Experiment 2 should be interpreted in much the same manner as those of condition C<sub>1</sub>C<sub>2</sub>|C<sub>1</sub>C<sub>2</sub> in Experiment 1. That is, in quadrants 1 and 3, the modulation of orientation components add their contributions to an overall contrast modulation, in quadrants 2 and 4 the contributions cancel. Thus, the involvement of an isotropic FRF mechanism would express itself in terms of lower thresholds in quadrants 1 and 3 compared to those in quadrants 2 and 4. This asymmetry of thresholds is apparent for all observers in Experiment 2a (solid symbols) where only relevant (modulated) orientation bands were present in the textures. Thus, it appears that in Experiment 2a isotropic FRF mechanisms did play a significant role in task performance. However, in Experiment 2b thresholds are much more similar between the quadrants, suggesting that an isotropic FRF mechanism did not play a significant role in task performance here. The  $p$ -values associated with the model fits generally confirm these conclusions. Whereas with only a few exceptions, the three-mechanism model provides excellent fits to the data of both Experiment 2a and 2b, the two-mechanism model tends to fit well only the data of experiment 2b.

Overall, these results are in line with what one would expect from the idea that texture processing is mediated by a process of probability summation among two standard FRF mechanisms and an isotropic FRF mechanism. In Experiment 2a, textures contained only contrast in the relevant (i.e., modulated) orientation bands and an isotropic FRF mechanism would be especially well-equipped to detect a modulation of overall contrast if it exists. In Experiment 2b, however, textures also contained contrast energy

in irrelevant (i.e., unmodulated) orientation bands. This manipulation would be especially detrimental to the performance of the isotropic FRF mechanism since it integrates first-order information not only across the relevant but also the irrelevant channels. The standard FRF mechanisms would be relatively unaffected by the presence of contrast energy in irrelevant, unmodulated orientation bands since these mechanisms 'look' only in relatively narrow orientation channels. Performance in Experiment 2b would thus be expected to be dominated by probability summation among the two standard FRF mechanisms, as is found to be the case.

#### 4. Summary of results and general discussion

In a series of two experiments, textures were created by combining contrast modulations in two distinct orientation bands. In Experiment 1, the spectral composition of the textures and in particular that of the modulated sidebands mimicked those found in a more or less natural context, namely that of an orientation modulation. However, in the experiment the modulations of contrasts in the two sidebands were manipulated independently. Depending on the specific combination of modulation amplitudes in the two sidebands, the texture displayed either a modulation in overall contrast or a modulation of overall (e.g., average) orientation.

It was found that, at least for some observers, contrast modulations in the two orientation sidebands interacted. Specifically, when the modulations were combined such that their contributions to a modulation in overall contrast added, the modulations were easier to detect compared to combinations in which the contributions to an overall contrast modulation cancelled. Results were well-described in terms of a model which assumes that performance is mediated by three mechanisms: two standard FRF mechanisms which detect contrast modulations within narrow orientation channels and an isotropic mechanism which detects modulations in contrast across all orientation. The three mechanisms appear to combine their efforts through probability summation. For most of the observers, however, results were also well-described by a model which assumes that performance is mediated by two standard FRF mechanisms only.

Experiment 2 was designed specifically to test the idea that three mechanisms underlie the detection of two simultaneous contrast modulations in distinct orientation bands. The textures utilized in Experiment 2 contained again contrast modulations in two distinct orientation bands with various relative modulation amplitudes. When the textures contained energy only in relevant (i.e., modulated) bands (Experiment 2a), the results were fit remarkably well with a model which assumes that performance is determined by probability summation among three mechanisms: two standard FRF mechanisms and one isotropic mechanism. A model which assumes probability summation between two standard FRF mechanisms did not provide an adequate fit for any of the observers.

When the texture contained energy also in irrelevant bands, however, the results were well-described also by the model which assumes the existence of standard FRF mechanisms only. This pattern of results is expected since an isotropic FRF mechanism integrates across all first-order orientations including those that are irrelevant.

It is important to note that the addition of contrast energy in irrelevant orientation bands did not simply deteriorate performance uniformly across the various angles  $\phi$ , but rather led to a distinctly different pattern of results. What this implies is that these results would be hard to explain in terms of standard FRF mechanisms only, by a process of, for example, masking or contrast normalization as this would affect performance equally for all angles  $\phi$ .

Generally, the model which assumes that performance is mediated by probability summation among two standard FRF mechanisms and an isotropic FRF mechanism describes the results remarkably well, especially when one considers that it has only four free parameters. Even where this model should be rejected based on the associated p-value (using our somewhat arbitrary but conventional 0.05 criterion), the model at least appears to capture the general pattern of thresholds quite well. The poor statistical fit in these cases might instead be caused by observer lapses. Lapses at high stimulus amplitudes would have a devastating effect on the likelihood of the best-fitting three-mechanism model, but would have a much lesser effect on the likelihood of the saturated model against which it is compared.

Isotropic FRF mechanisms similar to those discussed here have been proposed by [Motoyoshi and Kingdom \(2007\)](#). Motoyoshi and Kingdom propose that two streams of second-order visual processing exist, one stream consisting of standard FRF mechanisms, the other consisting of mechanisms that integrate across first-order orientations but are selective for first-order luminance polarity. Motoyoshi and Kingdom suggest that the latter type of model could also be involved in the detection of contrast modulations. This prediction is confirmed here.

As was shown in Experiment 2, the isotropic FRF mechanism is, predictably, much more affected by the presence of contrast in unmodulated channels compared to standard FRF mechanisms. However, it is more difficult to explain why the relative roles of standard and isotropic mechanisms differs between observers as demonstrated in the results of Experiment 1. The relative efficiency of standard FRF mechanisms can theoretically be improved by a retuning of the orientation tuning function of the first-order channels of these mechanisms. Such retuning of first-order response properties has been shown to result from training ([Saarinen & Levi, 1995](#); [Schoups, Vogels, Qian, & Orban, 2001](#); [Yang & Manusell, 2004](#)). Such retuning could improve the signal-to-noise ratio within standard FRF mechanisms by isolating the relevant, modulated channels before second-order filtering occurs. Texture segmentation has indeed been shown to be subject to perceptual learning ([Ahissar & Hochstein, 1993](#); [Ahissar & Hochstein, 1997](#); [Karni & Sagi, 1991](#); [Karni & Sagi, 1993](#)) though the specific mechanism by which this learning occurs has not yet been explained. A project is currently underway in our lab to investigate the role of first-order template retuning in perceptual learning of texture segmentation.

#### Acknowledgements

This paper has benefited significantly from comments on an earlier version by Michael Landy and an anonymous reviewer.

#### Appendix A

##### A.1. Model fits

The data of all Experiments were fit under two models. The 'two-mechanism model' assumes that performance is mediated by two standard FRF mechanisms, one of which detects contrast modulations in one of the modulated orientation channels, the other detects contrast modulations in the other modulated orientation channel. The characteristics of the first-order channels are as described in Sections 2.2 and 3.2 (For Experiments 1 and 2, respectively). Modulation amplitude  $A$  was transformed into  $M_1$ ,  $M_2$ , and  $M_{iso}$  as described in Section 2.2. The probability of detection for each of the two standard FRF mechanisms was assumed to be related to  $M_1$  and  $M_2$ , respectively, by way of the Weibull function. The two standard FRF mechanisms were assumed to have

equal parameters of the psychometric function. Similarly, the probability of detection for the isotropic FRF mechanisms was assumed to be related to  $M_{iso}$  by way of the Weibull function.

Mechanisms combine their efforts by way of probability summation. That is, if at least one of the mechanisms detects a modulation, the observer responds correctly. If none of the mechanisms detects a modulation, the observer guesses. The probability of a correct response under the two-mechanism model then is:

$$p(M_1, M_2; \alpha_{st}, \beta_{st}) = \lambda + (1 - \lambda) \times (1 - (1 - \psi_W(M_1; \alpha_{st}, \beta_{st})) \times (1 - \psi_W(M_2; \alpha_{st}, \beta_{st}))) \quad (A.1)$$

where  $M_1$  and  $M_2$  are as above,  $\alpha_{st}$  and  $\beta_{st}$  are the common threshold contrast modulation and the common slope of the two standard FRF mechanisms,  $\lambda$  is a guessing parameter which was fixed at 0.5, and  $\psi_W$  symbolizes the Weibull function:

$$\psi_W(x; \alpha, \beta) = 1 - \exp\left(-\left(\frac{x}{\alpha}\right)^\beta\right) \quad (A.2)$$

This model thus has only two free parameters: a common threshold ( $\alpha_{st}$ ) and a common slope ( $\beta_{st}$ ) for the standard FRF mechanisms. Best-fitting estimates for these parameters were obtained by the Nelder-Mead search algorithm using a maximum likelihood criterion.

The 'three-mechanism model' fitted to the data was similar to that described above except that performance was assumed to be mediated by probability summation among three mechanisms: the two standard FRF mechanisms as in the two-mechanism model but now also an isotropic mechanism which detects modulations in overall contrast. If at least one of the three mechanisms detects a modulation, the observer responds correctly. If none of the mechanisms detects a modulation, the observer guesses. The probability of a correct response then is:

$$p(M_1, M_2, M_{iso}; \alpha_{st}, \beta_{st}, \alpha_{iso}, \beta_{iso}) = \lambda + (1 - \lambda) \times (1 - (1 - \psi_W(M_1; \alpha_{st}, \beta_{st})) \times (1 - \psi_W(M_2; \alpha_{st}, \beta_{st})) \times (1 - \psi_W(M_{iso}; \alpha_{iso}, \beta_{iso}))) \quad (A.3)$$

where  $M_1, M_2, M_{iso}, \alpha_{st}, \beta_{st}, \lambda$ , and  $\psi_W$  are as above,  $\alpha_{iso}$  is the threshold of the psychometric function relating probability of detection in the isotropic mechanism to  $M_{iso}$ , and  $\beta_{iso}$  is the slope of this function. This model has four free parameters: a common threshold and slope for the two standard FRF mechanisms ( $\alpha_{st}$  and  $\beta_{st}$ ), and a threshold and a slope for the isotropic FRF mechanisms ( $\alpha_{iso}$  and  $\beta_{iso}$ ).

### A.2. Goodness-of-fit

In order to determine goodness-of-fit, a likelihood ratio test (e.g., Hoel, Port & Stone; 1971) was used. The likelihood ratio test compares the fit of two models statistically. The two-mechanism model and the three-mechanism model were both compared against the 'saturated' model. The saturated model has no parametric constraints on the probability of a correct response for any amplitude/angle  $\phi$  combination in the experiment. Rather, it estimates a probability of correct response for each of these unique conditions individually. For each observer in each experiment, the three models (two-mechanism, three-mechanism, and the saturated model) were fitted to the data using a maximum likelihood criterion (Section A.1). Deviance values (which are transformations of the Likelihood ratio; e.g., Wichmann & Hill, 2001) were then calculated for both the two- and three-mechanism model fits as, respectively:

$$D_2 = 2(LL_{Sat}(\hat{\rho}|\mathbf{y}) - LL_2(\hat{\alpha}_{st}, \hat{\beta}_{st}|\mathbf{y})) \quad (A.4)$$

$$D_3 = 2(LL_{Sat}(\hat{\rho}|\mathbf{y}) - LL_3(\hat{\alpha}_{st}, \hat{\beta}_{st}, \hat{\alpha}_{iso}, \hat{\beta}_{iso}|\mathbf{y})) \quad (A.5)$$

where  $LL_{Sat}(\hat{\rho}|\mathbf{y})$  is the log likelihood of the saturated model,  $\hat{\rho}$  is the set of maximum likelihood estimates of the probability of correct detection for each modulation amplitude/angle  $\phi$  combination in the experiment, and  $\mathbf{y}$  is the set of observed responses,  $LL_2(\hat{\alpha}_{st}, \hat{\beta}_{st}|\mathbf{y})$  is the log likelihood of the two-mechanism model using maximum likelihood estimates of  $\alpha_{st}$  and  $\beta_{st}$ , and  $LL_3(\hat{\alpha}_{st}, \hat{\beta}_{st}, \hat{\alpha}_{iso}, \hat{\beta}_{iso}|\mathbf{y})$  is the log likelihood of the three-mechanism model using maximum likelihood estimates of  $\alpha_{st}, \beta_{st}, \alpha_{iso}$ , and  $\beta_{iso}$ .

Deviance values obtained from the data of the observer were then compared against sampling distributions of Deviance values obtained by Monte Carlo simulations. Empirical sampling distributions of  $D_2$  values were obtained by repeatedly ( $B = 4000$ ) simulating an observer that acts in accordance with the constraints of the two-mechanism model above using the maximum likelihood estimates for  $\alpha_{st}$  and  $\beta_{st}$  obtained from the human data. In the simulations the same number of trials and stimulus amplitudes were used as in the human observer's experiment (since stimulus amplitudes were determined by an adaptive method, these stimulus values differed from observer to observer). Deviance values were then calculated for each of the simulated experiments (Eq. (A.4)). The distribution of these Deviance values then served as the sampling distribution against which the Deviance based on the human observer's data was compared. The  $p_2$ -values listed in the figures are the proportion of simulated data sets for which the Deviance value was greater compared to the Deviance value obtained from the human observer.

The  $p_3$  values listed were derived in an analogous manner. That is, the data of the observer were fitted with the three-mechanism model and a  $D_3$  value was calculated (Eq. (A.5)). An observer was then simulated which acted according to the best-fitting three-mechanism model to the human observer's data ( $B = 4000$ ). The distribution of simulated  $D_3$  values served as the empirical sampling distribution against which the  $D_3$  value obtained from the human observer was compared.

It should be noted that in Experiment 1 not all three-mechanism fits to the simulated data converged successfully (all two-mechanism fits to simulated data in Experiment 1 converged successfully as did all fits in Experiment 2). Not all simulated data-sets were fit successfully by the three-mechanism model in the following observer/condition combinations in Experiment 1: NP 0|C<sub>1</sub>C<sub>2</sub> (3999 of 4000 [ $\sim 100.0\%$ ] converged), NP C<sub>1</sub>|C<sub>2</sub> (99.6%), NP C<sub>1</sub>C<sub>2</sub>|C<sub>1</sub>C<sub>2</sub> (99.6%), JR 0|C<sub>1</sub>C<sub>2</sub> (99.7%), JR C<sub>1</sub>|C<sub>2</sub> (99.9%), JR C<sub>1</sub>C<sub>2</sub>|C<sub>1</sub>C<sub>2</sub> (97.5%), and MJM C<sub>1</sub>C<sub>2</sub>|C<sub>1</sub>C<sub>2</sub> (99.9%). In these conditions, p-values were calculated based on the fits that did successfully converge. Theoretically this is not a proper method, of course. However, given the very small proportion of failed fits there is hardly any practical significance to them.

The most likely reason for the (few) failed simulated model fits is that the fitting procedure attempts to find estimates of the parameters of both the standard and the isotropic FRF mechanisms. However, in all of the above conditions the isotropic mechanism appeared to play a very minor role in human (and thus also the simulated) performance. As the isotropic mechanism did not have much of an effect on the simulated data, these simulated data would consequently not contain much information regarding the parameters of this mechanism.

### A.3. The component added vs. subtracted asymmetry deconstructed

It is demonstrated here how the component *added* versus component *subtracted* asymmetry in thresholds in Experiment 1 condition 0|C<sub>1</sub>C<sub>2</sub> arises. In general, the pattern of predicted thresholds based on the three-mechanism model in this condition (as well as in condition C<sub>1</sub>|C<sub>2</sub>) is asymmetric with respect to the left diagonal in the result graphs. The asymmetry is especially apparent in the results of KD. Interestingly, the observed thresholds actually

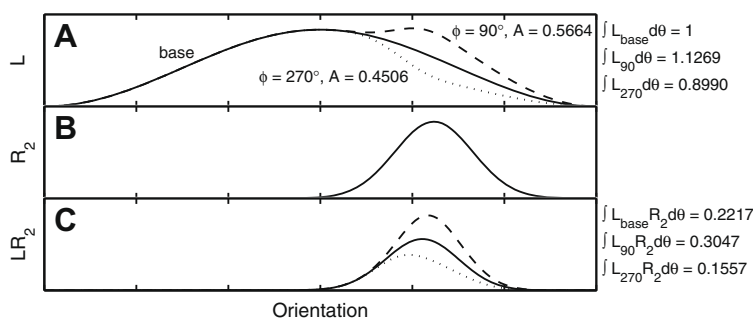


Fig. 12. Derivation of  $M_{\text{channel}}$  and  $M_{\text{iso}}$  values for the example discussed in Section A.3.

follow the predicted asymmetry quite closely. In order to understand the mechanism behind this asymmetry, let us have a close look at the textures corresponding to KD's thresholds for angle  $\phi = 90^\circ$  (texture bars containing base only are alternated with bars in which one sideband component is added to base spectrum) and angle  $\phi = 270^\circ$  (texture bars containing base only are alternated with bars in which one sideband component is subtracted from base spectrum).

Consider Fig. 12, which shows the amplitude spectra across orientation for these two conditions (A), the modeled channel of a standard FRF mechanism which is centered on the modulated sideband (B) and the signal available within this channel (C) in a fashion analogous to Fig. 7. At angle  $\phi = 90^\circ$ , one of the texture regions contains only the base texture (solid lines), the alternate texture regions contain base texture plus the contrast in the modulated sideband (broken lines). At angle  $\phi = 270^\circ$ , regions with spectra corresponding to the solid lines (base) are alternated with regions corresponding to the dotted lines (base minus modulated sideband). Plotted in Fig. 8a are the predicted thresholds in terms of signal available to a standard FRF mechanism only ( $M_{\text{channel}}$ ).  $M_{\text{channel}}$  at angle  $\phi = 90^\circ$  equals  $M_{\text{channel}} = (.3047 - .2217) / (.3047 + .2217) = 0.1577$ . Similarly at angle  $\phi = 270^\circ$ ,  $M_{\text{channel}} = (.1557 - .2217) / (.1557 + .2217) = -0.1749$ . Note that the observed thresholds mimic the asymmetry quite closely.

The asymmetry is readily explained by considering the signal available to the isotropic mechanism. The signal available to the isotropic mechanism is greater for the stimulus at angle  $\phi = 90^\circ$  [ $M_{\text{iso}} = (1.1269 - 1) / (1.1269 + 1) = 0.0597$ ] compared to that at angle  $\phi = 270^\circ$  [ $M_{\text{iso}} = (0.8990 - 1) / (0.8990 + 1) = -0.0532$ ]. Thus, whereas the standard FRF mechanism would, of course, perform less well with the threshold texture at angle  $\phi = 90^\circ$  compared to that at angle  $\phi = 270^\circ$  (after all,  $M_{\text{channel}}$  is lower), the isotropic mechanism does better with this stimulus ( $M_{\text{iso}}$  is greater). In other words, the role played by the isotropic mechanism, relative to the standard FRF mechanism, at angle  $\phi = 90^\circ$  is greater than it is at angle  $\phi = 270^\circ$ . The reasoning applied here can be generalized to angles  $\phi$  at which both sidebands are modulated.

## Appendix B. Supplementary data

Supplemental figures show example textures for all of the conditions in both experiment 1 and 2. Textures are shown at angle  $\phi = 0^\circ, 45^\circ, 90^\circ, \dots, 315^\circ$ . Textures are arranged in correspondence to angle  $\phi$ . Angle  $\phi$  is also noted in each texture. Note that in Figures S.1c (condition  $C_1C_2|C_1C_2$ , Experiment 1), S.2a (Experiment 2a) and S.2b (Experiment 2b) each texture lists two angles  $\phi$  as in these conditions angles  $\phi$  and  $\phi + 180^\circ$  correspond to equivalent textures. Supplementary data associated with this article can be found, in the online version, at doi:10.1016/j.visres.2008.09.005.

## References

- Ahissar, M., & Hochstein, S. (1993). Attentional control of early perceptual learning. *Proceedings of the National Academy of Science, USA*, 90, 5718–5722.
- Ahissar, M., & Hochstein, S. (1997). Task difficulty and the specificity of perceptual learning. *Nature*, 387, 401–406.
- Campbell, F. W., Cooper, G. F., & Enroth-Cugell, C. (1969). The spatial selectivity of the visual cells of the cat. *Journal of Physiology*, 203, 223–235.
- Cutting, J. E., & Millard, R. T. (1984). Three gradients and the perception of flat and curved surfaces. *Journal of Experimental Psychology: General*, 113, 198–216.
- Dakin, S. C., & Mareschal, I. (2000). Sensitivity to contrast modulation depends on carrier spatial frequency and orientation. *Vision Research*, 40, 311–329.
- DeValois, R. L., & DeValois, K. K. (1988). *Spatial Vision*. Oxford, UK: Oxford University Press.
- Efron, B., & Tibshirani, R. J. (1993). *An introduction to the bootstrap*. Boca Raton, FL: Chapman & Hall/CRC.
- Graham, N., & Sutter, A. (1998). Spatial summation in simple (Fourier) and complex (non-Fourier) texture channels. *Vision Research*, 38, 231–257.
- Graham, N., Sutter, A., & Venkatesan, C. (1993). Spatial-frequency and orientation-selectivity of simple and complex channels in region segregation. *Vision Research*, 33, 1893–1911.
- Graham, N., & Wolfson, S. S. (2004). Is there opponent-orientation coding in the second-order channels of pattern vision? *Vision Research*, 44, 3145–3175.
- Hoel, P. G., Port, S. C., & Stone, C. J. (1971). *Introduction to statistical theory*. Boston, MA: Houghton Mifflin Company.
- Hubel, D. H., & Wiesel, T. N. (1962). Receptive fields, binocular interaction and functional architecture in the cat's visual cortex. *Journal of Physiology*, 160, 106–154.
- Jamar, J. H. T., & Koenderink, J. J. (1985). Contrast detection and detection of contrast modulation for noise gratings. *Vision Research*, 25, 511–521.
- Karni, A., & Sagi, D. (1991). Where practice makes perfect in texture discrimination: Evidence for primary visual cortex plasticity. *Proceedings of the National Academy of Science, USA*, 88, 4966–4970.
- Karni, A., & Sagi, D. (1993). The time course of learning a visual skill. *Nature*, 365, 250–252.
- Knill, D. C. (1998a). Discrimination of planar surface slant from texture: Human and ideal observers compared. *Vision Research*, 38, 1683–1711.
- Knill, D. C. (1998b). Ideal observer perturbation analysis reveals human strategies for inferring surface orientation from texture. *Vision Research*, 38, 2635–2656.
- Kontsevich, L. L., & Tyler, C. W. (1999). Bayesian adaptive estimation of psychometric slope and threshold. *Vision Research*, 39, 2729–2737.
- Landy, M. S., & Bergen, J. R. (1991). Texture segregation and orientation gradient. *Vision Research*, 31, 679–691.
- Langley, K., Fleet, D. J., & Hibbard, P. B. (1996). Linear filtering precedes nonlinear processing in early vision. *Current Biology*, 6, 891–896.
- Li, A., & Zaidi, Q. (2000). Perception of three-dimensional shape from texture is based on patterns of oriented energy. *Vision Research*, 40, 217–242.
- Li, A., & Zaidi, Q. (2001). Information limitations in perception of shape from texture. *Vision Research*, 41, 1519–1533.
- Li, A., & Zaidi, Q. (2003). Observer strategies in perception of 3-D shape from isotropic textures: Developable surfaces. *Vision Research*, 43, 2741–2758.
- Malik, J., & Perona, P. (1990). Preattentive texture discrimination with early vision mechanisms. *Journal of the Optical Society of America A*, 7, 923–932.
- Mareschal, I., & Baker, C. L. (1998). A cortical locus for the processing of contrast-defined contours. *Nature Neuroscience*, 1, 150–154.
- Mareschal, I., & Baker, C. L. (1999). Cortical processing of second-order motion. *Visual Neuroscience*, 16, 527–540.
- Motoyoshi, I., & Kingdom, F. A. A. (2007). Differential roles of contrast polarity reveal two streams of second-order visual processing. *Vision Research*, 47, 2047–2054.
- Motoyoshi, I., & Nishida, S. (2004). Cross-orientation summation in texture segregation. *Vision Research*, 44, 2567–2576.
- Prins, N., & Kingdom, F. A. A. (2002). Orientation- and frequency-modulated textures at low depths of modulation are processed by off-orientation and off-frequency texture mechanisms. *Vision Research*, 42, 705–713.

- Prins, N., & Kingdom, F. A. A. (2003). Detection and discrimination of texture modulations defined by orientation, spatial frequency, and contrast. *Journal of the Optical Society of America A*, 20, 401–410.
- Prins, N., & Kingdom, F. A. A. (2006). Direct evidence for the existence of energy-based texture mechanisms. *Perception*, 35, 1035–1046.
- Rosas, P., Wichmann, F. A., & Wagemans, J. (2004). Some observations on the effects of slant and texture type on slant-from-texture. *Vision Research*, 44, 1511–1535.
- Saarinen, J., & Levi, D. M. (1995). Perceptual learning in Vernier acuity: What is learned? *Vision Research*, 35, 519–527.
- Schoups, A., Vogels, R., Qian, N., & Orban, G. (2001). Practicing orientation identification improves orientation coding in V1 neurons. *Nature*, 412, 549–553.
- Sutter, A., Sperling, G., & Chubb, C. (1995). Measuring the spatial frequency selectivity of second-order texture mechanisms. *Vision Research*, 35, 915–924.
- Treisman, A. (1985). Preattentive processing in vision. *Computer Vision, Graphics, and Image Processing*, 31, 156–177.
- Wichmann, F. A., & Hill, N. J. (2001). The psychometric function: I. Fitting, sampling, and goodness of fit. *Perception & Psychophysics*, 63, 1293–1313.
- Yang, T., & Maunsell, J. H. R. (2004). The effect of perceptual learning on neuronal responses in monkey visual area V4. *The Journal of Neuroscience*, 24, 1617–1626.